

Deconfined criticality at the onset of antiferromagnetism in a metal

Ya-Hui Zhang and Subir Sachdev

Department of Physics, Harvard University, Cambridge, MA 02138, USA

(Dated: May 15, 2022)

Abstract

We propose a general theoretical framework, using two layers of ancilla qubits, for a continuous transition between a Fermi liquid with a large Fermi surface, and a pseudogap metal with a small Fermi surface of electron-like quasiparticles. The pseudogap metal can be a magnetically ordered metal, or a fractionalized Fermi liquid (FL*) without magnetic order. A ‘ghost’ Fermi surface emerges (alongside the large electron Fermi surface) at the quantum critical point, with the ghost fermions carrying neither spin nor charge, but minimally coupled to $(U(1) \times U(1))/Z_2$ or $(SU(2) \times U(1))/Z_2$ gauge fields. Away from the critical point on the pseudogap side, the ghost Fermi surface absorbs part of the large electron Fermi surface, and leads to a jump in the Hall co-efficient. We also find an example of an “unnecessary quantum critical point” between a metal with spin density order, and a metal with local moment magnetic order. The ghost fermions contribute a $T \ln(1/T)$ specific heat at temperature T at the critical point, and could also be detected in other thermal probes. We relate our results to the phases of correlated electron compounds.

CONTENTS

I. Introduction	3
II. Ancilla qubits and gauge symmetries	6
III. Mean field theories	9
A. FL*	9
B. AF Metal	11
C. SDW Metal	12
IV. Kondo lattice	13
V. Structure of Critical Theories	15
A. Lattice symmetry	16
1. DQCP1	16
2. DQCP2	16
3. DQCP3	17
B. Action for ghost fermions Ψ	17
1. DQCP1	17
2. DQCP2 and DQCP3	17
C. Action for Higgs bosons Φ	18
1. DQCP1	18
2. DQCP2	19
3. DQCP3	19
VI. Critical ghost Fermi surfaces	20
A. Stability of the ghost Fermi surface at $m = 0$	20
B. Instability of the ghost Fermi surface at $m^2 > 0$	23
C. Phase diagram	24
VII. Higgs boson fluctuations	25
A. Universal conductivity	26
VIII. Property of the Physical Fermi surface	28
IX. Conclusions	28
Acknowledgements	30

A. RG flow of the ghost Fermi surface coupled to a $U(1) \times U(1)$ gauge field	30
B. Pairing instability for the FL*-FL transition with $U(2)$ gauge theory	33
1. Pairing instability	34
C. Relation to Hertz-Millis theory	35
References	36

I. INTRODUCTION

The study of the quantum phase transition involving the onset of antiferromagnetic order in metals is a central topic in modern quantum condensed matter theory. There are applications to numerous materials, including the f -electron ‘heavy fermion’ compounds [1–6], the cuprates [7–9], and the ‘115 compounds’ [10, 11]. The standard theory involves a Landau-Ginzburg-Wilson approach, obtaining an effective action for the antiferromagnetic order parameter damped by the low energy Fermi surface excitations [3, 12, 13]. However, a number of experiments, especially in quasi-two dimensional compounds, do not appear to be compatible with this approach [7, 14–16].

In this paper, we shall present a ‘deconfined critical theory’ [17, 18], involving fractionalized excitations and gauge fields at a critical point, flanked by phases with only conventional excitations. Such a scenario for the metallic antiferromagnetic critical point has been discussed earlier [5], but no specific critical theory was proposed. Reviews of related ideas are in Refs. 19–21. We note that a deconfined critical theory for the onset of spin glass order in a metal was obtained recently [22] in a model with all-to-all random couplings. There will be no randomness in the models we consider here, and only short-range couplings.

Our theory relies on the recently introduced [23] ‘ancilla qubit’ approach to correlated electron systems. In addition to the ‘physical layer’ corresponding to the lattice Hamiltonian of the system of interest, we introduce two ‘hidden layers’ of ancilla qubits (see Fig. 1). By entangling the physical degrees of freedom with the ancilla, and then projecting out a trivial product state of the ancilla qubits, we are able to access a rich variety of quantum phases and critical points for the physical layer. In this manner we obtain here a deconfined theory of the onset for the antiferromagnetic order in a metal with (i) additional ‘ghost’ Fermi surfaces at the critical point of fermions that carry neither spin nor charge; (ii) a jump in the size of the Fermi surfaces with the electron-like quasiparticles which carry both spin and charge, and a correspondingly discontinuous Hall effect; (iii) a logarithmic enhancement of the linear in temperature specific heat at the critical point.

As we will review in Section II, the ancilla approach leads to a parent $(SU(2)_S \times SU(2)_1 \times SU(2)_2)/Z_2$ gauge theory. The Higgs/confining phases, and intervening critical points or phases,

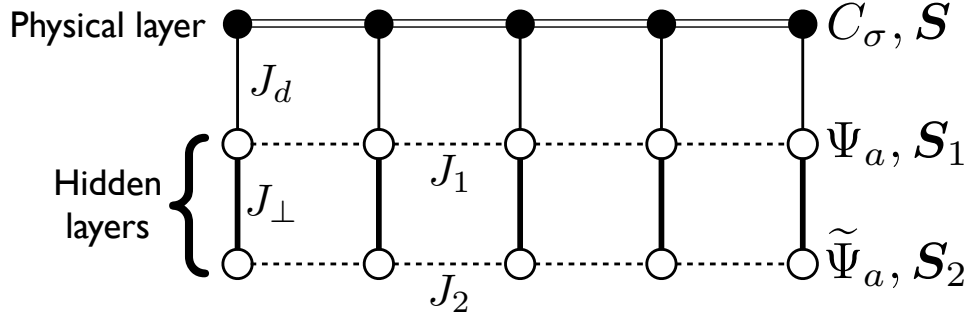


FIG. 1. The top layer is the physical layer coupled to two ‘hidden’ layers of ancilla qubits (spin-1/2 spins) $\mathcal{S}_{i;1}$ and $\mathcal{S}_{i;2}$. The physical layer is taken to be either a single band model of electrons $C_{i;\sigma}$, or a Kondo lattice of electrons $C_{i;\sigma}$ coupled to a separate set of spins \mathcal{S} . The lattice sites are labeled by i , and can form any d -dimensional lattice (only one dimension is displayed above), and $\sigma = \uparrow, \downarrow$ is a physical spin index. We develop a theory with the exchange interactions finite, and take the limit $J_{\perp} \rightarrow \infty$ of infinite antiferromagnetic exchange between the hidden layers at the end. This leads to a $(SU(2)_S \times SU(2)_1 \times SU(2)_2)/Z_2$ gauge theory, with all gauge symmetries acting on the hidden layers. The hidden layers are described by ‘ghost fermions’ $\Psi_{i;a}, \tilde{\Psi}_{i;a}$ which carry neither spin nor charge; $a = +, -$ is a $SU(2)_S$ gauge index.

of this gauge theory lead to many interesting phase diagrams of correlated electron systems. We emphasize that, unlike previous gauge theories in the literature, the electron operator in the physical layer is not fractionalized, and remains gauge neutral. All the gauge symmetries act only on the hidden layers, but we are also able to reproduce earlier results in which gauge charges resided in the physical layer. A crucial advantage of the ancilla approach is that it is far easier to keep track of Fermi surfaces, and the constraints arising from generalizations of the Luttinger constraint of Fermi liquid theory [24, 25]. In particular, this approach led to [23] the first self-contained description of the transformation from a fractionalized Fermi liquid (FL*) with a small Fermi surface, to a regular Fermi liquid (FL) with a large Fermi surface in a single band model, with the correct Fermi surface volumes at mean-field level in both phases. (The FL* phase has no symmetry breaking, and the violation of the conventional Luttinger constraint by its small Fermi surface is accounted for by the presence of fractionalized excitations and bulk topological order [24–26].) The critical theory (labeled DQCP1 below) had a Fermi surface of ghost fermions and a Higgs field both carrying fundamental $(SU(2)_S \times U(1)_1)/Z_2$ gauge charges. We note the recent work of Refs. 27 and 28 which described metal-insulator transition or metal-metal transition using $U(2)$ or $U(1) \times U(1)$ gauge theories, but not using the ancilla method.

We will present our results in the context of the global phase diagram presented in Fig. 2. In addition to the FL and FL* phases noted above, it shows two types of metals with antiferromagnetic

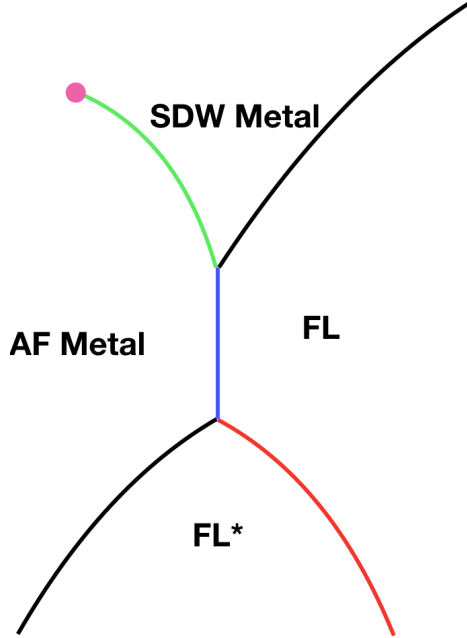


FIG. 2. A global phase diagram obtained from our ancilla qubit approach. The red, blue, green lines are three different deconfined critical theories described in the present paper: DQCP1, DQCP2 and DQCP3. DQCP1 is the FL*-FL transition. DQCP2 is the transition between AF Metal and the symmetric FL. DQCP3 is a transition within AF Metal. The DQCP3 may have an end point (denoted as a solid circle) after which the transition becomes a crossover. The FL-SDW Metal transition in a conventional transition in the Hertz-Millis class [12, 13], and the FL*-AF Metal transition is described by a QED₃ model discussed briefly in Section III B.

(Néel) order: the AF Metal and the SDW Metal. These are both ‘conventional’ phases without excitations carrying charges of emergent gauge fields, and there is no fundamental distinction between them. Nevertheless the underlying physical interpretations of these phases is quite distinct. The SDW Metal arises from the appearance of a weak spin density wave in a FL state, and the consequent reconstruction of the Fermi surface. On the other hand, the AF Metal can be considered as arising from a ‘Kondo breakdown’ transition [19, 24, 29], where local moments appear due to absence of Kondo screening in the environment. These two pictures can lead to different Fermi surface shapes and topologies, but (apart from Fermi surface reconnections) the SDW Metal and AF Metal can be continuously connected, as indicated in Fig. 2.

Our analysis will lead to a sharper delineation of the distinction between the SDW Metal and AF Metal phases. As indicated in Fig. 2 the universality class of the phase transition from the FL to the AF Metal is distinct from the universality class of the transition from the FL to the SDW Metal: we will show that the first is described by a deconfined $(U(1)_S \times U(1)_1)/Z_2$ gauge theory,

while the latter is in the conventional Hertz-Millis class [12, 13]. Another example of deconfined critical point for Landau symmetry breaking transition has been proposed in Ref. 30, but it does not involve a Fermi surface.

Another surprising result in Fig. 2 is the presence of a sharp phase transition between the SDW Metal and the AF Metal, over a certain range of parameters. This is an example of an ‘unnecessary’ quantum phase transition [31], and will be described in our case by deconfined $(U(1)_S \times U(1)_1)/Z_2$ gauge theory.

The mean field structure of the phases of Fig. 2 will be described in Section III. Here we will use a single band model for the physical layer. Section IV will extend the mean field theory to a Kondo lattice in the physical layer, leading to very similar results.

We will begin description of the 3 DQCPs in Fig. 2 in Section V, by a description of their overall and gauge and symmetry structures. The critical theories have three sectors of matter fields: a bosonic critical Higgs sector, a ghost Fermi surface coupled to different gauge fields, and a Fermi surface of gauge-neutral electrons in the physical layer. We will first consider the critical ghost Fermi surface sector in Section VI. This will be followed by a consideration of the Higgs sector in Section VII, and the physical Fermi surface of electrons in Section VIII.

II. ANCILLA QUBITS AND GAUGE SYMMETRIES

We begin by reviewing basic aspects of the ancilla qubit approach [23], and the associated $(SU(2)_S \times SU(2)_1 \times SU(2)_2)/Z_2$ gauge symmetry.

Let $\mathbf{S}_{i,1}$, $\mathbf{S}_{i,2}$ be the spin operators acting on the qubits in the two hidden layers, where i is a lattice site (see Fig. 1). We can represent these spin operators with hidden fermions $F_{i,\sigma}$, $\tilde{F}_{i,\sigma}$ via

$$\mathbf{S}_{i,1} = \frac{1}{2} F_{i,\sigma}^\dagger \boldsymbol{\sigma}_{\sigma\sigma'} F_{i,\sigma'} \quad , \quad \mathbf{S}_{i,2} = \frac{1}{2} \tilde{F}_{i,\sigma}^\dagger \boldsymbol{\sigma}_{\sigma\sigma'} \tilde{F}_{i,\sigma'} \quad (2.1)$$

where $\boldsymbol{\sigma}$ are the Pauli matrices. Let us also define the Nambu pseudospin operators

$$\begin{aligned} \mathbf{T}_{i,1} &= \frac{1}{2} \left(F_{i,\downarrow}^\dagger F_{i,\uparrow}^\dagger + F_{i,\uparrow} F_{i,\downarrow}, i \left(F_{i,\downarrow}^\dagger F_{i,\uparrow}^\dagger - F_{i,\uparrow} F_{i,\downarrow} \right), F_{i,\uparrow}^\dagger F_{i,\uparrow} + F_{i,\downarrow}^\dagger F_{i,\downarrow} - 1 \right) \\ \mathbf{T}_{i,2} &= \frac{1}{2} \left(\tilde{F}_{i,\downarrow}^\dagger \tilde{F}_{i,\uparrow}^\dagger + \tilde{F}_{i,\uparrow} \tilde{F}_{i,\downarrow}, i \left(\tilde{F}_{i,\downarrow}^\dagger \tilde{F}_{i,\uparrow}^\dagger - \tilde{F}_{i,\uparrow} \tilde{F}_{i,\downarrow} \right), \tilde{F}_{i,\uparrow}^\dagger \tilde{F}_{i,\uparrow} + \tilde{F}_{i,\downarrow}^\dagger \tilde{F}_{i,\downarrow} - 1 \right). \end{aligned} \quad (2.2)$$

For a more transparent presentation of the symmetries, it is useful to write the fermions as 2×2 matrices

$$\mathbf{F}_i = \begin{pmatrix} F_{i,\uparrow} & -F_{i,\downarrow}^\dagger \\ F_{i,\downarrow} & F_{i,\uparrow}^\dagger \end{pmatrix}. \quad (2.3)$$

This matrix obeys the relation

$$\mathbf{F}_i^\dagger = \sigma^y \mathbf{F}_i^T \sigma^y. \quad (2.4)$$

We use a similar representation for $\tilde{\mathbf{F}}$. Now we can write the spin and Nambu pseudospin operators as

$$\begin{aligned}\mathbf{S}_{i;1} &= \frac{1}{4}\text{Tr}(\mathbf{F}_i^\dagger \boldsymbol{\sigma} \mathbf{F}_i) \\ \mathbf{T}_{i;1} &= \frac{1}{4}\text{Tr}(\mathbf{F}_i^\dagger \mathbf{F}_i \boldsymbol{\sigma}),\end{aligned}\tag{2.5}$$

and similarly for $\mathbf{S}_{i;2}$ and $\mathbf{T}_{i;2}$ with $\tilde{\mathbf{F}}$.

We now describe the gauge symmetries obtained by transforming to rotating reference frames in both spin and Nambu pseudospin spaces [32–34]. Note that in the ancilla approach [23], the gauge symmetries act only on the hidden layers, and we leave the degrees of freedom in the physical layer intact and gauge-invariant. We introduce the ‘rotated’ gauge-charged fermions $\Psi_i, \tilde{\Psi}_i$ in the hidden layers via

$$\mathbf{F}_i = L_i \Psi_i R_i \quad , \quad \tilde{\mathbf{F}}_i = \tilde{L}_i \tilde{\Psi}_i \tilde{R}_i\tag{2.6}$$

where L, R, \tilde{L} and \tilde{R} are 2×2 $SU(2)$ matrices, and the Ψ fermions have a decomposition similar to (2.3)

$$\Psi_i = \begin{pmatrix} \Psi_{i;+} & -\Psi_{i;-}^\dagger \\ \Psi_{i;-} & \Psi_{i;+}^\dagger \end{pmatrix}.\tag{2.7}$$

We use indices $a = +, -$ for $\Psi_{i;a}$ rather than \uparrow, \downarrow in (2.7) because the indices are not physical spin in the rotated reference frame. Again an analogous representation for $\tilde{\Psi}_{ia}$ is used. For the spin and Nambu pseudospin operators, (2.6) implies the transformation (and correspondingly for $S_{i;2}^\alpha$ and $T_{i;2}^\alpha$)

$$S_{i;1}^\alpha = \mathcal{L}_i^{\alpha\beta} \frac{1}{4}\text{Tr}(\Psi_i^\dagger \tau^\beta \Psi_i)\tag{2.8}$$

$$T_{i;2}^\alpha = \mathcal{R}_i^{\alpha\beta} \frac{1}{4}\text{Tr}(\Psi_i^\dagger \tilde{\Psi}_i \tau^\beta)\tag{2.9}$$

where $\alpha, \beta = x, y, z$ and τ^β are Pauli matrices; we are using τ^β rather than σ^β here to signify that these matrices act on the rotated $a = +, -$ indices. The $\mathcal{L}_i, \mathcal{R}_i$ are 3×3 $SO(3)$ rotation matrices corresponding to the 2×2 $SU(2)$ rotations:

$$\begin{aligned}\mathcal{L}_i^{\alpha\beta} &= \frac{1}{2}\text{Tr}\left(L_i^\dagger \sigma^\alpha L_i \tau^\beta\right) \\ \mathcal{R}_i^{\alpha\beta} &= \frac{1}{2}\text{Tr}\left(R_i \sigma^\alpha R_i^\dagger \tau^\beta\right).\end{aligned}\tag{2.10}$$

Note that the spin operator transforms only under the L rotation, while the Nambu pseudospin operator only under the R rotation.

We now describe the gauge symmetries associated with the R_i and \tilde{R}_i . These are 2 copies of the $SU(2)$ gauge symmetries deployed in Ref. 32, which we denote here as $SU(2)_1$ and $SU(2)_2$ for

the layers. Note that the Nambu pseudospin in (2.8) transforms non-trivially under these gauge symmetries, and we wish to work in the gauge singlet sector. So, as in Ref. 32 for the physical layer, we impose constraints on the hidden layers,

$$\mathbf{T}_{i;1} = 0 \quad , \quad \mathbf{T}_{i;2} = 0 , \quad (2.11)$$

which restrict each site of the hidden layers to single occupancy of the $\Psi, \tilde{\Psi}$ fermions. It is useful to tabulate the action of the $SU(2)_1$ and $SU(2)_2$ symmetries on the fermions $\Psi, \tilde{\Psi}$ and the bosons $L, R, \tilde{L}, \tilde{R}$; we drop the site index i , as it is common to all fields:

$$\begin{aligned} SU(2)_1 : \quad & \Psi \rightarrow \Psi U_1 \quad , \quad \tilde{\Psi} \rightarrow \tilde{\Psi} \\ & R \rightarrow U_1^\dagger R \quad , \quad \tilde{R} \rightarrow \tilde{R} \\ & L \rightarrow L \quad , \quad \tilde{L} \rightarrow \tilde{L} \\ SU(2)_2 : \quad & \Psi \rightarrow \Psi \quad , \quad \tilde{\Psi} \rightarrow \tilde{\Psi} U_2 \\ & R \rightarrow R \quad , \quad \tilde{R} \rightarrow U_2^\dagger \tilde{R} \\ & L \rightarrow L \quad , \quad \tilde{L} \rightarrow \tilde{L} . \end{aligned} \quad (2.12)$$

Here, the gauge transformations are the $SU(2)$ matrices U_1 and U_2 respectively.

We have to follow a somewhat different approach for the gauge transformations associate with the rotations $L_{i;a}$. Now, we do *not* wish to impose the analog of the constraints (2.11) in the spin sector, because we don't want vanishing spin on each site of both layers. Rather, we want to couple the layers into spin singlets for each i , corresponding to the $J_\perp \rightarrow \infty$ limit in Fig. 1. This is achieved by the constraints

$$\mathbf{S}_{i;1} + \mathbf{S}_{i;2} = 0 . \quad (2.13)$$

We will impose the constraints (2.13) at a finite bare gauge coupling, because we do want to allow for some virtual fluctuations into the triplet sector at each i ; otherwise, the hidden layers would completely decouple from the physical layer at the outset. In contrast, (2.11) is imposed at an infinite bare gauge coupling [32]. In practice, the value of the bare gauge coupling makes little difference, because we will deal with a renormalized long time theory.

The mechanism for imposing (2.13) is straightforward. We transform to a common rotating frame in both layers by identifying

$$\begin{aligned} \tilde{L}_i &= L_i \\ \tilde{\mathcal{L}}_i &= \mathcal{L}_i . \end{aligned} \quad (2.14)$$

Now we have only a single $SU(2)_S$ gauge symmetry, related to that in Refs. 33–35, and the analog

of (2.12) is

$$\begin{aligned}
SU(2)_S : \quad \Psi &\rightarrow U_S \Psi \quad , \quad \tilde{\Psi} \rightarrow U_S \tilde{\Psi} \\
R &\rightarrow R \quad , \quad \tilde{R} \rightarrow \tilde{R} \\
L &\rightarrow LU_S^\dagger,
\end{aligned} \tag{2.15}$$

where U_S is $SU(2)$ matrix.

In summary, the crucial transformations for the subsequent development are those of the fermions Ψ , which we collect here:

$$\begin{aligned}
SU(2)_1 : \quad \Psi &\rightarrow \Psi U_1 \quad , \quad \tilde{\Psi} \rightarrow \tilde{\Psi} \\
SU(2)_2 : \quad \Psi &\rightarrow \Psi \quad , \quad \tilde{\Psi} \rightarrow \tilde{\Psi} U_2 \\
SU(2)_S : \quad \Psi &\rightarrow U_S \Psi \quad , \quad \tilde{\Psi} \rightarrow U_S \tilde{\Psi}.
\end{aligned} \tag{2.16}$$

The reader need only keep track of (2.16) for the following sections: the structure of all our effective actions is mainly dictated by the requirements of the gauge symmetries acting on the fermions in (2.16), and on the Higgs fields that will appear in the different cases. The Z_2 divisor in the overall $(SU(2)_1 \times SU(2)_2 \times SU(2)_S)/Z_2$ gauge symmetry arises from the fact that centers of the two $SU(2)$ transformations in (2.6) are the same.

III. MEAN FIELD THEORIES

We will begin by presenting some simple mean field theories of the $(SU(2)_S \times SU(2)_1 \times SU(2)_2)/Z_2$ gauge in the context of a one band model for the Hamiltonian of the physical layer. We will consider the extension to Kondo lattice models in Section IV, and find that the phenomenology remains essentially the same.

Our discussion will take place in the context of the schematic global phase diagram in Fig. 2. The general strategy will be to break the $(SU(2)_S \times SU(2)_1 \times SU(2)_2)/Z_2$ gauge symmetry by a judicious choice of Higgs fields, and then examine the fluctuations of the Higgs fields that become critical at the boundaries between the phases.

A. FL*

We first recall [23] the mean field theory for the FL* phase. As we will see below this FL* phase will act as a ‘parent’ phase for the other phases in Fig. 2.

We represent the electrons in the physical layer by C_σ , using a notation following the convention in Section II. As we noted earlier, we will not fractionalize C_σ directly: so the C_σ does not carry

any emergent gauge charges, only the global charges of the electromagnetic $U(1)_{em}$ and the spin rotation $SU(2)$. The FL* phase described by the following schematic Hamiltonian

$$H_* = H_C + H_\Psi + H_{\tilde{\Psi}} + \sum_i \left(C_{i;\sigma}^\dagger \Phi_{i;\sigma a} \Psi_{i;a} + \text{H.c.} \right), \quad (3.1)$$

where i is a lattice site index, $\sigma = \uparrow, \downarrow$ is a physical spin index, and $a = +, -$ is a gauge $SU(2)_S$ index. The Hamiltonian H_C is a generic one-band Hamiltonian for the electrons C_σ (a specific form appears in (3.4), with $N_0 = 0$ in the FL* state). The Hamiltonian for the first hidden layer, H_Ψ , is a spin liquid Hamiltonian which breaks $SU(2)_1$ down to $U(1)_1$; at its simplest this could be a free fermion Hamiltonian with a trivial projective symmetry group (PSG) so that the Ψ fermions on their own form a Fermi surface which occupies half the Brillouin zone (because the Ψ density is at half-filling, from (2.11)). Similarly, the Hamiltonian for the second hidden layer, $H_{\tilde{\Psi}}$, is a spin liquid Hamiltonian which breaks $SU(2)_2$ down to $U(1)_2$; however now we use the ‘staggered-flux’ ansatz [32], so that $\tilde{\Psi}$ excitations are Dirac fermions. (Specific forms for H_Ψ and $H_{\tilde{\Psi}}$ appear later in (3.3), with $M_{1,2} = 0$ in the FL* state).

The crucial term in (3.1) is the Higgs field $\Phi_{\sigma a}$, which is a 2×2 complex matrix linking the physical electrons to the first hidden layer. We will find it convenient to represent this by as pair of complex spinors Φ_a , with

$$\Phi_+ = \begin{pmatrix} \Phi_{\uparrow+} \\ \Phi_{\downarrow+} \end{pmatrix}, \quad \Phi_- = \begin{pmatrix} \Phi_{\uparrow-} \\ \Phi_{\downarrow-} \end{pmatrix} \quad (3.2)$$

From this representation, and the form of (3.1), it is clear that the Φ_a transform as follows under the various symmetries

- Φ_+ and Φ_- transform separately as fundamentals under the global $SU(2)$ spin rotation.
- Φ_a also carries the global electromagnetic $U(1)_{em}$ charge, with $\Phi_a \rightarrow e^{i\theta} \Phi_a$ and $C \rightarrow e^{i\theta} C$ under a global $U(1)_{em}$ rotation.
- Φ_a transforms as a fundamental under the $SU(2)_S$ gauge transformation, $\Phi_a \rightarrow \Phi_b [U_S^\dagger]_{ba}$, while, as in (2.16), $\Psi_a \rightarrow [U_S]_{ab} \Psi_b$ and $\tilde{\Psi}_a \rightarrow [U_S]_{ab} \tilde{\Psi}_b$.
- Φ_a carries the $U(1)_1$ gauge charge, with $\Phi_a \rightarrow e^{-i\vartheta_1} \Phi_a$, along with $\Psi_a \rightarrow e^{i\vartheta_1} \Psi_a$.
- Φ_a is neutral under the $U(1)_2$ gauge charge, with $\Phi_a \rightarrow \Phi_a$, while $\tilde{\Psi}_a \rightarrow e^{i\vartheta_2} \tilde{\Psi}_a$.

The FL* phase arises when Φ_a is condensed. Then, the above transformations make it clear that both $SU(2)_S$ and $U(1)_1$ are fully broken (or ‘higgsed’). The electromagnetic $U(1)_{em}$ is however preserved because there is no gauge-invariant operator carrying $U(1)_{em}$ charge which acquires an

expectation value. The condensation of Φ_a effectively ties $U(1)_1$ to $U(1)_{em}$ (this is as in the usual ‘slave particle’ theories). Similarly, if we choose $\Phi_{\sigma a} \propto \delta_{\sigma a}$ spin rotation invariance is preserved, and a becomes like an effective global spin index.

The properties of such a FL* phase were discussed in some detail in Ref. 23. The C and Ψ fermions are hybridized to form small pockets with total Fermi surface volume $A_{FS} = p/2$, where the electron density in the physical layer is $1 - p$. It is quite natural to expect that only Fermi arcs are visible in ARPES measurement while the backside of the pocket is dominated by Ψ and has very small spectral weight in terms of the physical electron C . Because the $SU(2)_S$ gauge field is locked to the external physical spin gauge field, the other ghost fermion $\tilde{\Psi}$ now becomes a neutral spinon and forms a $U(1)$ Dirac spin liquid.

We will consider phase transitions out of this FL* phase later in this paper. In particular, the FL*-FL transition (see Fig. 2) is described by a theory of the vanishing of the Higgs condensate $\langle \Phi_a \rangle$ while spin rotation is preserved. This yields a critical theory, denoted DQCP1 in Fig. 2, in which the key degrees of freedom are the bosons Φ_a and the Ψ Fermi surface coupled to $SU(2)_S \times U(1)_1$ gauge fields; the structure of the effective action can be deduced from the symmetry and gauge transformations we have described above. We will find in Section VI that such a Ψ Fermi surface is unstable to pairing, and FL*-FL transition likely occurs via an intermediate phase.

B. AF Metal

Next, we consider the AF Metal phase in Fig. 2. This is a phase in spin rotation invariance is broken by antiferromagnetic order, and all the gauge fields are confined. We wish to obtain this state via a ‘Kondo breakdown’ transition in which the spins are liberated to form an antiferromagnet, rather than a spin density wave instability of an electronic Fermi surface; the latter is denoted SDW Metal in Fig. 2, and will be treated in Section III C. So we propose an effective Hamiltonian which perturbs the Hamiltonian H_* of the FL* phase in (3.1). The key idea is that the driving force for the appearance of antiferromagnetism in an AF Metal is the breaking of $SU(2)_S$ rather than global spin rotation symmetry; as $SU(2)_S$ is tied to global spin in the FL* phase, spin rotation symmetry will be broken as a secondary consequence. So the Hamiltonians of the 2 hidden layers, *i.e.* the ghost fermions, are as follows:

$$\begin{aligned}
 H_{\Psi} &= -t_{\Psi} \sum_{\langle ij \rangle} \Psi_i^{\dagger} \Psi_j - t'_{\Psi} \sum_{\langle\langle ij \rangle\rangle} \Psi_i^{\dagger} \Psi_j - M_1 \sum_i (-1)^i \Psi_i^{\dagger} \tau^z \Psi_i \\
 H_{\tilde{\Psi}} &= -t_{\tilde{\Psi}} \sum_{\langle ij \rangle} \tilde{\Psi}_i^{\dagger} \tilde{\Psi}_j + M_2 \sum_i (-1)^i \tilde{\Psi}_i^{\dagger} \tau^z \tilde{\Psi}_i
 \end{aligned} \tag{3.3}$$

As in Section II, we use τ^{α} ($\alpha = x, y, z$) to represent Pauli matrices acting the $SU(2)_S$ gauge symmetry space; we use σ^{α} to represent Pauli matrices acting of the global spin rotation space.

The new ingredients in (3.3), not present in the FL* phase, are the Higgs fields $M_{1,2}$ which break $SU(2)_S$ gauge symmetry down to $U(1)_S$. The presence of M_2 will gap out the $\tilde{\Psi}$ Dirac fermions, and so $U(1)_2$ will confine. Recall that the $\langle\Phi_a\rangle$ condensate has already completely broken the $SU(2)_S$ and $U(1)_1$ gauge symmetries. So there are no remaining free gauge charges, and we obtain a conventional phase with global $SU(2)$ spin rotation symmetry broken down to $U(1)$.

In considering the phase transition from the AF Metal to the FL phase in Fig. 2 (labeled DQCP2), we consider the vanishing of the Higgs field Φ_a , while $M_{1,2}$ remain non-zero. Then we obtain a critical theory which is very similar to the FL*-FL theory discussed above, except that the gauge symmetry is only $U(1)_S \times U(1)_1$ *i.e.* the main ingredients are the bosons Φ_a and the Ψ_a Fermi surface coupled to $U(1)_S \times U(1)_1$ gauge fields. Note, however, that the global spin rotation invariance will be restored at the critical point, because spin rotation was only broken via the Φ_a condensate.

We will show in Section VI that this AF Metal-FL theory has an important difference from the FL*-FL theory: it is now possible to have a stable critical Ψ_a Fermi surface which does not pair. Once we move to the other side of the critical point, and the Higgs fields are gapped, then the pairing instability does set in, and we expect a crossover to a confining phase which is likely to be a conventional FL state.

Let us also consider the FL*-AF Metal transition shown in Fig. 2. Starting from the FL* state, this transition is realized by turning on a M_2 condensate, while the Φ_a condensate remains non-zero. Then, within the second hidden layer, the critical properties are described by a model considered earlier [36–39]: an O(3) QED₃ Gross-Neveu-Yukawa model. The spectator FL* Fermi surfaces could have a significant influence on this conformal field theory, but we will not explore this here. We also note other approaches to the FL*-AF Metal transition [40, 41], with different spin liquid structures in the FL* phase.

C. SDW Metal

Now we consider the SDW Metal of Fig. 2: this is conventional SDW Metal, obtained as an instability of the large Fermi surface of the electrons C_σ . So now we directly break the spin rotation symmetry by a C_σ bilinear, in contrast to the indirect breaking via the ghost fermion bilinears in (3.3) for the AF Metal. So the Hamiltonian H_C in H_* becomes

$$H_C = - \sum_{i,j} t_{ij} C_i^\dagger C_j + N_0 \sum_i (-1)^i C_i^\dagger \sigma^z C_i \quad (3.4)$$

where N_0 is proportional to the physical antiferromagnetic order. We note that as long as there is a Φ_a Higgs condensate, there is no fundamental distinction between the N_0 symmetry breaking in

(3.4), and the $M_{1,2}$ Higgs condensates of the AF Metal in (3.3). Both eventually lead to the same phase: a ‘trivial’ phase with no emergent gauge charges, and long-range antiferromagnetic order. The distinction is only a question of degree. In the SDW Metal, N_0 is the primary driving force, and drives the appearance of the $M_{1,2}$ condensates as a secondary consequence, while the opposite is true in the AF Metal. Nevertheless, there can be significant observable differences in the shapes and topologies of the Fermi surfaces, with those of the SDW Metal arising from a reconstruction of the large Fermi surface of the C fermions.

Furthermore, we will show that there can be a novel ‘unnecessary phase transition’ [30, 31] between the AF Metal and the SDW Metal, denoted DQCP3 in Fig. 2. The critical theory for this transition is very similar to that of the AF Metal-FL transition discussed above. The only distinction is that the global spin rotation symmetry is reduced from $SU(2)$ to $U(1)$: so we again obtain a theory of bosons Φ_a and the Ψ Fermi surface coupled to $U(1)_S \times U(1)_1$ gauge fields.

IV. KONDO LATTICE

Before turning to a consideration of the deconfined phase transitions in Fig. 2, this section will extend the mean field considerations to the case where the physical layer is a Kondo lattice model. The microscopic model was already illustrated in Fig. 1; we consider

$$\begin{aligned}
H &= H_K + H_1 + H_2 + H_{S1} + H_{12} \\
H_K &= -t \sum_{\langle ij \rangle} C_i^\dagger C_j + J_K \sum_i (C_i^\dagger \boldsymbol{\sigma} C_i) \cdot \mathbf{S}_i + J \sum_{\langle ij \rangle} \mathbf{S}_i \cdot \mathbf{S}_j \\
H_1 &= J_1 \sum_{\langle ij \rangle} \mathbf{S}_{j;1} \cdot \mathbf{S}_{j;1} \quad , \quad H_2 = J_2 \sum_{\langle ij \rangle} \mathbf{S}_{i;2} \cdot \mathbf{S}_{j;2} \\
H_{12} &= J_\perp \sum_i \mathbf{S}_{i;1} \cdot \mathbf{S}_{i;2} \quad , \quad H_{S1} = J_d \sum_i \mathbf{S}_i \cdot \mathbf{S}_{i;1}
\end{aligned} \tag{4.1}$$

Above $C_{i\sigma}$ is the itinerant electron, \mathbf{S}_i is the local moment; $\mathbf{S}_{i;1}$ and $\mathbf{S}_{i;2}$ are the spins in the hidden layers. We will take $J_\perp \rightarrow \infty$ limit to recover the standard Kondo-Heisenberg model.

We perform the conventional heavy-fermion mean field theory on the physical layer, and the parton description described in Section II on the hidden layers. The physical layer is represented by a 2-band model involving hybridization between the electrons $C_{i\alpha}$ and the $f_{i\sigma}$ fermions used to represent the Kondo lattice spins \mathbf{S}_i , and the hidden layers are represented by the mean field theory for $\Psi, \tilde{\Psi}$ described in Section III. So, our mean field theory is:

$$\begin{aligned}
H_M &= H_{c,f} + H_\Psi + H_{\text{Higgs}} + H_{\tilde{\Psi}} \\
H_{c,f} &= -t_c \sum_{\langle ij \rangle} C_i^\dagger C_j - t_f \sum_{\langle ij \rangle} f_i^\dagger f_j - t'_f \sum_{\langle\langle ij \rangle\rangle} f_i^\dagger f_j - t''_f \sum_{\langle\langle ij \rangle\rangle} f_i^\dagger f_j + K \sum_i (C_i^\dagger f_i + \text{H.c.}) \quad , \tag{4.2}
\end{aligned}$$

and H_Ψ and $H_{\tilde{\Psi}}$ are as in (3.3). Finally we need to add the Higgs term to describe the Kondo breaking down

$$H_{\text{Higgs}} = \sum_i \left(f_{i;\sigma}^\dagger \Phi_{i;\sigma a} \Psi_{i;a} + \text{H.c.} \right), \quad (4.3)$$

similar to that (3.1). If both $M_{1,2}$ and Φ_a are non-zero, then the physical spin rotation symmetry is broken, and we obtain a AF Metal state with Néel order.

We always assume the Kondo coupling $K \neq 0$, and therefore f can also be viewed as physical electron. The Kondo breakdown happens when we add $\Phi \neq 0$. (This is to be compared with a theory of the FL*-FL transition in a Kondo lattice model [24, 26], where Kondo breakdown occurred via the vanishing of the Higgs field representing the Kondo coupling K .) With large Φ , f will be tightly bound with Ψ and both disappear in the low energy. This is exactly what we expect from the picture that f gets Mott localized. In the low energy there is still degree of freedom from $\tilde{\Psi}$, which can now be viewed as a spinon for the localized moment after Mott localization. Because of the ansatz we assumed for $H_{\tilde{\Psi}}$, these local moments form a Neel order. In summary, the final state is a small pocket formed by C moving on top of Neel order formed by localized moment. This picture is different from a SDW Metal, although there is no sharp distinction in terms of symmetry and topology.

In Fig. 3 we show plots of single electron spectrum after the transition of condensing $\langle \Phi_{\sigma a} \rangle = \Phi \delta_{\sigma a}$. We use $t_c = 10$, $t_f = 1$, $t'_f = -0.1$, $t''_f = 0.1$, $t_\psi = -1$ and $t'_\psi = 0.1$. In our framework the Kondo coupling K is finite at the Kondo breaking down transition. But it is natural to expect that K is small at the quantum critical point, thus we use $K = 1$. At this value the heavy Fermi liquid have two separate pockets: one small Fermi surface mainly from c and one large one mainly from f , as shown in Fig. 3(a). When we add a small value of Φ , f and Ψ get hybridized and gapped after a small inter-mediate region. Here only $\Phi = 0.2$ is needed to fully gap out the Fermi surface formed by f . In our convention the hopping of the spinon is 1, which implies the energy scale of spin-spin interaction is at order of $1 - 10$. Thus $\Phi = 0.2$ is only a few percent of spin-spin interaction scale. The transition we are describing is a Kondo breaking down transition and Φ is associated with the charge gap and should be determined by Hubbard U . Therefore the region $\Phi < 0.2$ should be very small and in the real experiment one may see an almost abrupt destruction of the Fermi surface associated with f .

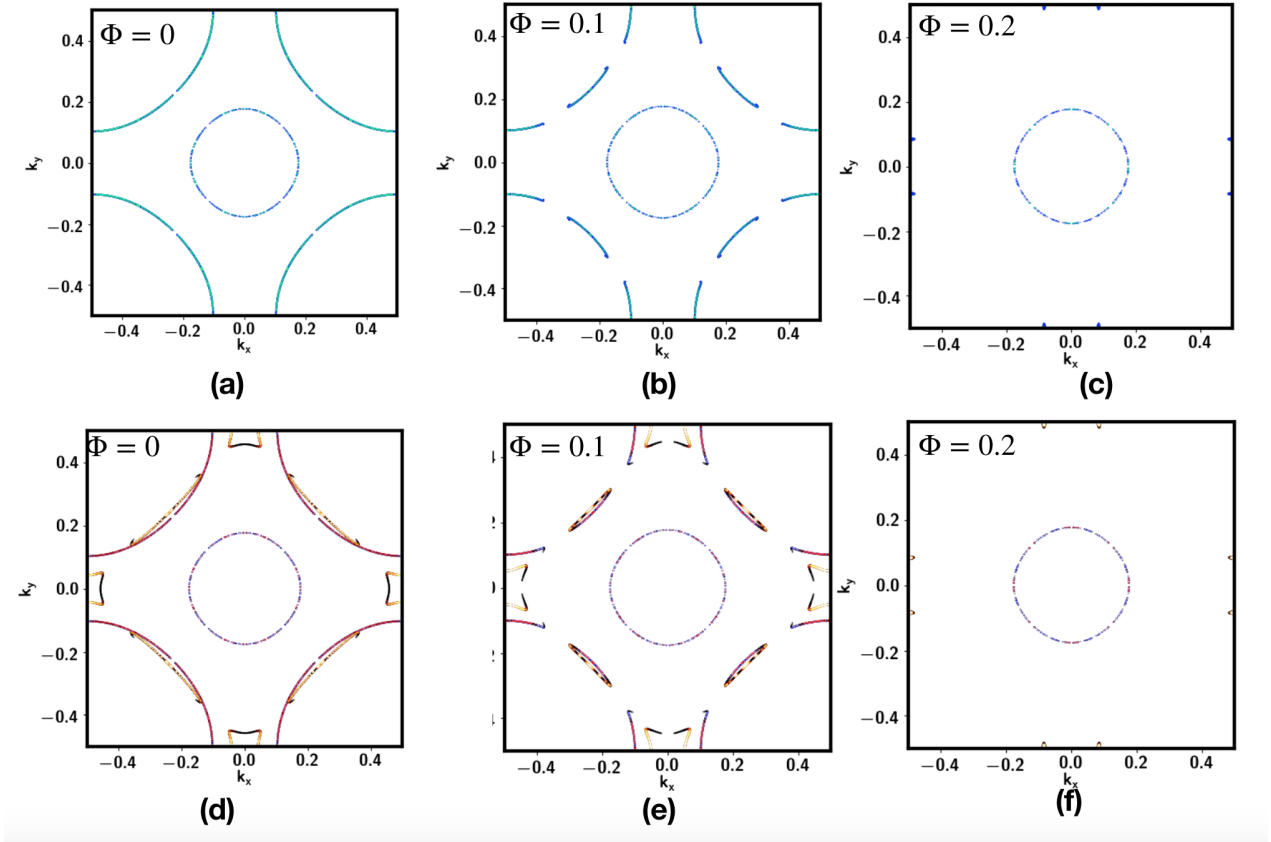


FIG. 3. Evolution of $A(\omega = 0, \mathbf{k})$ when increasing Φ . In the first row we plot $A_c(\omega = 0, \mathbf{k}) + A_f(\omega = 0, \mathbf{k})$. In the second row we further include the contribution from Ψ and plot $A_c(\omega = 0, \mathbf{k}) + A_f(\omega = 0, \mathbf{k}) + A_\Psi(\omega = 0, \mathbf{k})$.

V. STRUCTURE OF CRITICAL THEORIES

Our discussion in Section III of the phases of Fig. 2, also stated the ingredients of the effective theory of the critical points between them. All critical theories have the same important matter degrees of freedom: a 4-component complex scalar $\Phi_{a\sigma}$, and a Fermi surface of the 2-component complex fermions Ψ_a at half-filling. Both matter fields carry fundamental gauge charges, and are subject to different symmetry constraints. In summary, these are:

- DQCP1 between FL and FL* is described by a $(SU(2)_S \times U(1)_1)/Z_2$ gauge theory with a global $SU(2)$ spin rotation symmetry.
- DQCP2 between FL and AF Metal is described by a $(U(1)_S \times U(1)_1)/Z_2$ gauge theory with a global $SU(2)$ spin rotation symmetry.
- DQCP3 between AF Metal and SDW Metal is described by a $(U(1)_S \times U(1)_1)/Z_2$ gauge

theory with a global U(1) spin rotation symmetry.

In addition to these gauge and global symmetries, lattice and time reversal symmetries also play an important role. We discuss these, and the resulting effective actions for the fermions and bosons in the following subsections.

Generically, the Lagrangian for the critical theory has the following structure:

$$L = L_C + L_\Psi + L_\Phi + g \sum_{a=\pm} (C^\dagger \Phi_a) \Psi_a + L_{\Phi\Psi} + L_{\Phi C} \quad (5.1)$$

where L_C is the Lagrangian for the Fermi surface of C electrons in the physical layer, L_Φ is the Lagrangian for the Higgs field, and L_Ψ is the Lagrangian for the ghost fermion sector. Both Φ and Ψ couple to the internal gauge fields and we have suppressed the action for the gauge fields. The main communication between the physical sector C and the hidden sector Φ, Ψ is through the Yukawa coupling g in the above, but there are also terms in the form $(C^\dagger \sigma^\beta C)(\Phi^\dagger \tau^\alpha \sigma^\beta \Phi)$ included in $L_{\Phi C}$.

A. Lattice symmetry

The projective lattice symmetry plays an essential role in the critical theory for DQCP2 and DQCP3. Therefore we list the lattice symmetries first for the three DQCPs. We will only focus on the time reversal symmetry T and translation symmetry T_x, T_y .

1. DQCP1

For DQCP1, the lattice symmetry transforms trivially.

$$\begin{aligned} T: \quad C &\rightarrow i\sigma^y C, \quad \Psi \rightarrow \Psi, \quad \Phi \rightarrow i\sigma^y \Phi \\ T_x: \quad C &\rightarrow C, \quad \Psi \rightarrow \Psi, \quad \Phi \rightarrow \Phi \\ T_y: \quad C &\rightarrow C, \quad \Psi \rightarrow \Psi, \quad \Phi \rightarrow \Phi \end{aligned} \quad (5.2)$$

Here we suppress the transformation of the coordinate (x, y) of the field. T always transforms (x, y) to (x, y) . T_x transforms (x, y) to $(x + 1, y)$ and T_y transforms (x, y) to $(x, y + 1)$.

2. DQCP2

For DQCP2, the translation symmetry needs to act projectively to keep the ansatz (3.3) invariant. Because of the M_1 term, we need to add a gauge transformation $i\tau^y \in SU(2)_S$ after T_x and

T_y .

$$\begin{aligned}
T &: C \rightarrow i\sigma^y C, \quad \Psi \rightarrow \Psi, \quad \Phi \rightarrow i\sigma^y \Phi \\
T_x &: C \rightarrow C, \quad \Psi \rightarrow i\tau^y \Psi, \quad \Phi \rightarrow i\tau^y \Phi \\
T_y &: C \rightarrow C, \quad \Psi \rightarrow i\tau^y \Psi, \quad \Phi \rightarrow i\tau^y \Phi
\end{aligned} \tag{5.3}$$

3. DQCP3

For DQCP3, there is always a Neel order parameter as shown in Eq. 3.4. Both the time reversal symmetry and the translation symmetry are already broken. We are left with the combined symmetry $T_x T$ and $T_y T$.

$$\begin{aligned}
T_x T &: C \rightarrow i\sigma^y C, \quad \Psi \rightarrow i\tau^y \Psi, \quad \Phi \rightarrow -\tau^y \sigma^y \Phi \\
T_y T &: C \rightarrow i\sigma^y C, \quad \Psi \rightarrow i\tau^y \Psi, \quad \Phi \rightarrow -\tau^y \sigma^y \Phi
\end{aligned} \tag{5.4}$$

B. Action for ghost fermions Ψ

Here we introduce the Lagrangian L_Ψ in (5.1).

1. DQCP1

For the FL-FL* transition, Ψ couples to the $U(1)_1$ and $SU(2)_S$ gauge fields. We can ignore the $\tilde{\Psi}$ part, and the $U(1)_2$ gauge field, which are not touched across the transition. We label the $U(1)_1$ gauge field as a_1 and the $SU(2)_S$ gauge field as a_S . We have

$$L_\Psi = \Psi^\dagger (\partial_\tau - ia_{1;0} - ia_{S;0}^\alpha \tau^\alpha) \Psi - \frac{\hbar^2}{2m^*} \Psi^\dagger (\partial_i - ia_{1;i} - ia_{S;i}^\alpha \tau^\alpha)^2 \Psi + \dots \tag{5.5}$$

where $\alpha = x, y, z$ labels the three generators for the $SU(2)_S$ transformation. The ellipses denotes additional terms, including the four fermion interaction. Note that Ψ does not carry either physical spin or physical charge. The lattice symmetry acts trivially in this case.

2. DQCP2 and DQCP3

For DQCP2 and DQCP3, Ψ couples to a $(U(1)_1 \times U(1)_S)/Z_2$ gauge field. We label a_1 and a_S for $U(1)_1$ and $U(1)_S$ respectively. It is convenient to relabel $a_+ = a_1 + a_S$ and $a_- = a_1 - a_S$, then Ψ_+ couples to a_+ and Ψ_- couples to a_- . The low energy Lagrangian is of the form

$$L_\Psi = \sum_{a=\pm} \Psi_a^\dagger (\partial_\tau - ia_{a;0}) \Psi_a - \frac{\hbar^2}{2m^*} \sum_{a=\pm} \Psi_a^\dagger (\partial_i - ia_{a;i})^2 \Psi_a + \dots \tag{5.6}$$

On the square lattice, the M_1 term in Eq. 3.3 will reconstruct Ψ_a to have electron and hole pockets with the same size (the sum over pockets is not indicated above). But the Fermi surfaces for Ψ_+ and Ψ_- are always the same and inversion symmetric. Especially, there is perfect nesting for the pairing instability between Ψ_+ and Ψ_- .

C. Action for Higgs bosons Φ

Next we turn to the sector for the Higgs bosons, and Lagrangian L_Φ in (5.1), invariant under the symmetries in Section V A. In contrast to previous critical Higgs theories for the cuprates [35, 42–45] where the Higgs fields only carried gauge charges, here the Higgs fields also carry the physical electromagnetic and spin rotation quantum numbers. This has the important consequence that the Fermi surface induced Landau damping appears not in a term quadratic in the Higgs field (as in Refs. [35, 42]), but in the quartic term in L'_Φ to be discussed in Section VII.

1. DQCP1

$$L_\Phi = |(\partial_\mu - iA_\mu + ia_{1;\mu} + ia_{S;\mu}^\alpha \tau^\alpha)\Phi|^2 + m^2\Phi^\dagger\Phi + \tilde{\lambda}(\Phi^\dagger\Phi)^2. \quad (5.7)$$

$$+ \tilde{\lambda}_1(\Phi^\dagger\boldsymbol{\sigma}\Phi) \cdot (\Phi^\dagger\boldsymbol{\sigma}\Phi) + \tilde{\lambda}_2(\Phi^\dagger\boldsymbol{\tau}\Phi) \cdot (\Phi^\dagger\boldsymbol{\tau}\Phi) + \tilde{\lambda}_3 \sum_{\alpha,\beta=x,y,z} (\Phi^\dagger\tau^\alpha\sigma^\beta\Phi) \cdot (\Phi^\dagger\tau^\alpha\sigma^\beta\Phi)$$

where A_μ is a background gauge field, introduced as a source for the global electromagnetic $U(1)_{em}$ charge. There are 4 quartic terms invariant under gauge symmetries and those in Section V A, but they are not all linearly independent of each other. We can simplify the quartic terms by organizing them in the form $(\Phi_{a\sigma_1}^\dagger\Phi_{a\sigma_2})(\Phi_{b\sigma_3}^\dagger\Phi_{b\sigma_4})$, where $a, b = +, -$, and $\sigma_1, \sigma_2, \sigma_3, \sigma_4 = \uparrow, \downarrow$. By using the identities

$$\begin{aligned} (\Phi^\dagger\boldsymbol{\sigma}\Phi) \cdot (\Phi^\dagger\boldsymbol{\sigma}\Phi) &= (\Phi^\dagger\boldsymbol{\tau}\Phi)(\Phi^\dagger\boldsymbol{\tau}\Phi) \\ &= 2(\Phi_+^\dagger\boldsymbol{\sigma}\Phi_+) \cdot (\Phi_-^\dagger\boldsymbol{\sigma}\Phi_-) + \frac{1}{2}(\Phi^\dagger\Phi)^2 + \frac{1}{2}(\Phi^\dagger\tau_z\Phi)^2 \\ \sum_{\alpha,\beta=x,y,z} (\Phi^\dagger\tau^\alpha\sigma^\beta\Phi) \cdot (\Phi^\dagger\tau^\alpha\sigma^\beta\Phi) &= 2(\Phi^\dagger\Phi)^2 - (\Phi^\dagger\tau_z\Phi)^2 - 4(\Phi_+^\dagger\boldsymbol{\sigma}\Phi_+) \cdot (\Phi_-^\dagger\boldsymbol{\sigma}\Phi_-), \end{aligned} \quad (5.8)$$

we find the Lagrangian can be written with only two independent quartic couplings $\lambda_{1,2}$

$$L_\Phi = |(\partial_\mu - iA_\mu + ia_{1;\mu} + ia_{S;\mu}^\alpha \tau^\alpha)\Phi|^2 + m^2\Phi^\dagger\Phi + \lambda(\Phi^\dagger\Phi)^2 + \lambda_1(\Phi^\dagger\tau_z\Phi)^2 + 4\lambda_1(\Phi_+^\dagger\boldsymbol{\sigma}\Phi_+) \cdot (\Phi_-^\dagger\boldsymbol{\sigma}\Phi_-) \quad (5.9)$$

It is easy to notice that $\mathbf{n} = \Phi^\dagger\boldsymbol{\sigma}\Phi$ is gauge invariant and represents spin fluctuation at momentum $\mathbf{Q} = (0, 0)$.

2. DQCP2

For DQCP2, we have

$$L_\Phi = \sum_{a=\pm} |(\partial_\mu + ia_{a;\mu} - iA_\mu)\Phi_a|^2 + m^2 \sum_{a=\pm} |\Phi_a|^2 + \lambda \sum_{a=\pm} |\Phi_a|^4 + \lambda_1 |\Phi_+|^2 |\Phi_-|^2 + \lambda_2 (\Phi_+^\dagger \boldsymbol{\sigma} \Phi_+) \cdot (\Phi_-^\dagger \boldsymbol{\sigma} \Phi_-) \quad (5.10)$$

Because $(\Phi_a^\dagger \boldsymbol{\sigma} \Phi_a) \cdot (\Phi_a^\dagger \boldsymbol{\sigma} \Phi_a) = (\Phi_a^\dagger \Phi_a)^2$, there are no other quartic terms with the $SU(2)$ global spin rotation symmetry.

The action of the symmetries in Section VA allows us to define a set of intertwined order parameters from the $\Phi_{a\sigma}$. We can organize the order parameter as $O_{\alpha\beta} = \Phi^\dagger \tau^\alpha \sigma^\beta \Phi$, where τ^α are matrices in the gauged $SU(2)_S$ space with indices a, b , and σ^β are matrices in the global $SU(2)$ spin rotation space. To be gauge invariant, we need to restrict $\alpha = 0, z$, but β can be any one from $0, x, y, z$.

- $O_{00} = \Phi^\dagger \Phi$ corresponds to density fluctuation.
- $O_{z0} = \Phi^\dagger \tau^z \Phi = \Phi_+^\dagger \Phi_+ - \Phi_-^\dagger \Phi_-$ is a CDW order parameter with $\mathbf{Q} = (\pi, \pi)$.
- $\mathbf{n}_i^{\text{AF}} \sim (-1)^i \mathbf{S}_i \sim \Phi^\dagger \tau^z \boldsymbol{\sigma} \Phi = (\Phi_+^\dagger \boldsymbol{\sigma} \Phi_+ - \Phi_-^\dagger \boldsymbol{\sigma} \Phi_-)$ is the Neel order parameter.
- $\mathbf{n}_i^{\text{FM}} = \Phi^\dagger \boldsymbol{\sigma} \Phi = (\Phi_+^\dagger \boldsymbol{\sigma} \Phi_+ + \Phi_-^\dagger \boldsymbol{\sigma} \Phi_-)$ is a ferromagnetic (FM) order parameter.

One can easily check that T acts as $T : \mathbf{n}_i^{\text{AF}} \rightarrow -\mathbf{n}_i^{\text{AF}}$ and translation acts as $T_x : \mathbf{n}_i^{\text{AF}} \rightarrow -\mathbf{n}_{i+\hat{x}}^{\text{AF}}$. Meanwhile, $\mathbf{n}^{\text{FM}} \rightarrow -\mathbf{n}^{\text{FM}}$ under time reversal T and $\mathbf{n}^{\text{FM}} \rightarrow \mathbf{n}^{\text{FM}}$ under translation.

Because several intertwined order breaking have algebraic decay at the QCP, the exact symmetry breaking pattern at the $m^2 < 0$ side is selected by the quartic terms. For AF order, we need $\lambda_1 < 2\lambda$ and $\lambda_2 > 0$.

3. DQCP3

For DQCP3, the physical Neel order parameter will favor $\varphi_+ = \Phi_{+;\uparrow}$ and $\varphi_- = \Phi_{-;\downarrow}$. The $T_x T$ symmetry acts as $\varphi_+ \rightarrow -\varphi_-, \varphi_- \rightarrow \varphi_+$. The action reduces to:

$$L_\Phi = \sum_{a=\pm} |(\partial_\mu + ia_{a;\mu} - iA_\mu)\varphi_a|^2 + m^2 \sum_{a=\pm} |\varphi_a|^2 + \lambda \sum_{a=\pm} |\varphi_a|^4 + \lambda_1 |\varphi_1|^2 |\varphi_2|^2 \quad (5.11)$$

The AF order parameter is now $n_z^{\text{AF}} = \varphi_1^\dagger \varphi_1 + \varphi_2^\dagger \varphi_2$, while the FM order parameter is $n_z^{\text{FM}} = \varphi_1^\dagger \varphi_1 - \varphi_2^\dagger \varphi_2$. One can easily see that $\langle n_z^{\text{AF}} \rangle \neq 0$ for both $m^2 > 0$ and $m^2 < 0$, indicating a non-zero Neel order across the QCP.

VI. CRITICAL GHOST FERMI SURFACES

This section will consider the physics of the critical Fermi surfaces for the ghost Fermion Ψ in the DQCP theories introduced in Section V. Our approach will be to consider an effective action for the gauge fields, and then compute the consequences of these gauge fields on the ghost fermions near the Fermi surface. The effective action of the gauge fields will however be influenced by Higgs sector: it has a different form depending upon whether the Higgs mass $m^2 = 0$, as at the critical point, or in the massive Higgs phase, $m^2 > 0$, when the Higgs fields is not condensed.

One important consequence of the form of the gauge field action at $m^2 = 0$ is an enhancement of the linear-in- T specific heat of the Fermi surface. The critical fermion surface has a $T \ln(1/T)$ specific heat because the effective mass of Ψ has a log divergence due to the gauge field [46–48]. This appears to be compatible with experimental observations [49–51].

For DQCP2, it is possible that there are parameters where there are no ghost Fermi surfaces. In this case, the AF Metal-FL critical theory reduces to the Hertz-Millis [12, 13] theory, as we show in Appendix C. This demonstrates the crucial role played by the ghost Fermi surfaces in the deconfinement at the critical point.

The three theories presented in Section V are distinguished by the global spin rotation symmetry and the gauge fields. The global spin symmetry will not play any role in the present section. So the cases to consider are fermions coupled to $(SU(2)_S \times U(1)_1)/Z_2$ gauge fields, and to $(U(1)_S \times U(1)_1)/Z_2$ gauge fields. The ghost Fermi surface in DQCP1 with $(SU(2)_S \times U(1)_1)/Z_2$ gauge fields is argued to be unstable to pairing at zero magnetic field in Appendix B, implying an intermediate phase between FL and FL*. We will only consider the $(U(1)_S \times U(1)_1)/Z_2$ case here (as it is relevant to the AF Metal-FL DQCP2 transition of central interest, and to the DQCP3 transition), and describe the $(SU(2)_S \times U(1)_1)/Z_2$ case in Appendix B.

For the $(U(1)_S \times U(1)_1)/Z_2$ gauge theory, in the next two subsections we will describe conditions under which the ghost Fermi surface from Ψ is stable at the $m^2 = 0$ point, but is unstable to pairing with infinitesimal $m^2 > 0$. After the pairing $\langle \Psi_+ \Psi_- \rangle \neq 0$, the $(U(1)_S \times U(1)_1)/Z_2$ gauge field is higgsed down to $U(1)_S$, which then confines: this leads to the appearance of the FL phase for $m^2 > 0$. Our analysis will be based upon the renormalization group method of Ref. 48.

A. Stability of the ghost Fermi surface at $m = 0$

We analyze the stability of the QCP at $m = 0$. In this case, after a renormalization of the gauge field Lagrangian from polarization corrections from the fermions Ψ and bosons Φ , we obtain [48]:

$$L_a = \frac{1}{2} \left(\frac{1}{e_{c;0}^2} \mathbf{q}^2 + \frac{1}{e_c^2} |\mathbf{q}| + \kappa_0 \frac{|\omega|}{|\mathbf{q}|} \right) |a_1(\omega, \mathbf{q})|^2 + \frac{1}{2} \left(\frac{1}{e_{s;0}^2} \mathbf{q}^2 + \frac{1}{e_s^2} |\mathbf{q}| + \kappa_0 \frac{|\omega|}{\mathbf{q}} \right) |a_S(\omega, \mathbf{q})|^2 \quad (6.1)$$

Here the $|\omega|/|\mathbf{q}|$ terms are from Landau damping from the Ψ Fermi surfaces, and $e_{c;0}$ and $e_{s;0}$ are bare charges for Maxwell terms, which should depend on UV physics. We will always assume $e_{s;0} > e_{c;0}$. The $|\mathbf{q}|$ terms arise from the critical fluctuations of the Higgs boson [48]. We will assume in this subsection that

$$e_c^2 = e_s^2 = \frac{1}{\sigma_b v_b}, \quad (6.2)$$

where σ_b is the universal conductivity of the Higgs boson at the QCP and v_b is the velocity of the Higgs boson. The equality of the couplings in (6.2) relies on the equality of the Higgs boson conductivities associated with the $U(1)_S$ and $U(1)_1$ symmetries, and this is further discussed in Section VII A below. For DQCP3, the equality is immediate. For DQCP2, the equality depends upon the unknown fate of the quartic couplings $\lambda_{1,2}$ in (5.10) at the fixed point. If the fixed point of DQCP2 has a possible $O(8)$ symmetry (associated with the 8 real components of Φ , and the $O(8)$ symmetry of the kinetic terms), then the equality (6.2) follows. We show in Section VII A that any differences between the conductivities for DQCP2 arise only at order $\lambda_{1,2}^3$. From studies of the XY model, it is clear that such contributions are extremely small: in this case, the known conductivity [52–54] differs from the λ^0 term by only 10%.

Here we will show that the ghost Fermi surface can be stable even if $e_{s;0} > e_{c;0}$, provided there is a bare repulsive interaction between the fermions. The main point is that the bare Maxwell term is irrelevant at the critical point because the dominant kinetic energy for the gauge field $\sim |\mathbf{q}|$ is from the Higgs boson.

The leading contribution in BCS channel for ghost Fermi surface Ψ is from exchange of one photon. Generically, it is in the form

$$S_{BCS} = \int d^2k_i d\omega_i \Psi_a^\dagger(k_1) \Psi_b^\dagger(-k_1) \Psi_d(-k_2) \Psi_c(k_2) V_{ab} \delta_{ac} \delta_{bd} F(k_1 - k_2) \quad (6.3)$$

where $F(q = k_1 - k_2)$ arises from the propagator of the photons. The $\delta_{ac} \delta_{bd}$ factor is from the fact that the $U(1)_1$ and $U(1)_S$ interactions are diagonal in the (Ψ_+, Ψ_-) basis. For a_1 , we have $V_{11} = 1$, $V_{12} = 1$. For a_S , we have $V_{11} = 1$ and $V_{12} = -1$. This implies, as noted above, that a_S mediates attractive interaction between Ψ_+ and Ψ_- , while a_1 mediates repulsive interaction between Ψ_+ and Ψ_- . The final sign of the interaction between Ψ_+ and Ψ_- depends on the competition between a_1 and a_S .

We define dimensionless BCS interaction constant

$$\tilde{V}_m = \frac{k_F}{2\pi v_F} V_m \quad (6.4)$$

where m is the angular momentum for the corresponding pairing channel. By integrating photon

in the intermediate energy, we obtain [48]

$$\begin{aligned}
\delta\tilde{V}_m &= \frac{k_F}{2\pi v_F} v_F^2 \int \frac{d\theta}{2\pi} \left(\frac{e^{-im\theta}}{|k_F\theta|^2/e_{c;0}^2 + |k_F\theta|/e_c^2} - \frac{e^{-im\theta}}{|k_F\theta|^2/e_{s;0}^2 + |k_F\theta|/e_s^2} \right) \\
&= \frac{v_F}{4\pi^2} 2 \int_{\Lambda e^{-\delta\ell/2}}^{\Lambda} dq_y \left(\frac{1}{|q_y|^2/e_{c;0}^2 + |q_y|/e_c^2} - \frac{1}{|q_y|^2/e_{s;0}^2 + |q_y|/e_s^2} \right) \\
&= (\alpha_c - \alpha_s)\delta\ell - \left(\frac{\alpha_c e_c^2}{e_{c;0}^2} - \frac{\alpha_s e_s^2}{e_{s;0}^2} \right) \Lambda\delta\ell
\end{aligned} \tag{6.5}$$

where we have defined

$$\alpha_c = \frac{e_c^2 v_F}{4\pi^2}, \quad \alpha_s = \frac{e_s^2 v_F}{4\pi^2}. \tag{6.6}$$

We have also assumed that $e_c^2\Lambda/e_{c;0}^2 \ll 1$ and $e_s^2\Lambda/e_{s;0}^2 \ll 1$.

In Appendix A we find RG flow for α_c and α_s at the QCP:

$$\begin{aligned}
\frac{d\alpha_c}{d\ell} &= -\alpha_c(\alpha_c + \alpha_s) \\
\frac{d\alpha_s}{d\ell} &= -\alpha_s(\alpha_c + \alpha_s)
\end{aligned} \tag{6.7}$$

Because we expect $\alpha_c(\ell=0) = \alpha_s(\ell=0) = \frac{v_F}{4\pi^2\sigma_b v_b}$, we thus have $\alpha_c = \alpha_s$ at any RG time.

Next, let us consider the difference between the $U(1)_1$ and $U(1)_S$ sectors by defining the coupling

$$r = \left(\frac{\alpha_c e_c^2}{e_{c;0}^2} - \frac{\alpha_s e_s^2}{e_{s;0}^2} \right) \Lambda. \tag{6.8}$$

As shown in Appendix A, e_c and e_s do not flow, while the flows of α_c and α_s are only marginal [47, 48]. The couplings $1/e_{c;0}^2$ and $1/e_{s;0}^2$ terms are irrelevant from the naive scaling, and so we have

$$\frac{dr}{d\ell} = -r. \tag{6.9}$$

This RG equation should be combined with the flow of the BCS interaction obtained from (6.5), after setting $\alpha_c = \alpha_s$

$$\frac{dV}{d\ell} = -r - V^2. \tag{6.10}$$

Fig. 4 shows the RG flow of (6.9) and (6.10). There are two fixed points depending on the initial values. If the the initial value is in the left side of the red line, (r, V) flows to $(0, 0)$ and stops. This is a fixed point for the DQCP. If the initial value is in the right side of the red line, (r, V) will flow close to $(0, 0)$ but eventually escapes to $(0, -\infty)$. We will focus on the fixed point $(0, 0)$ for DQCP2 and DQCP3.

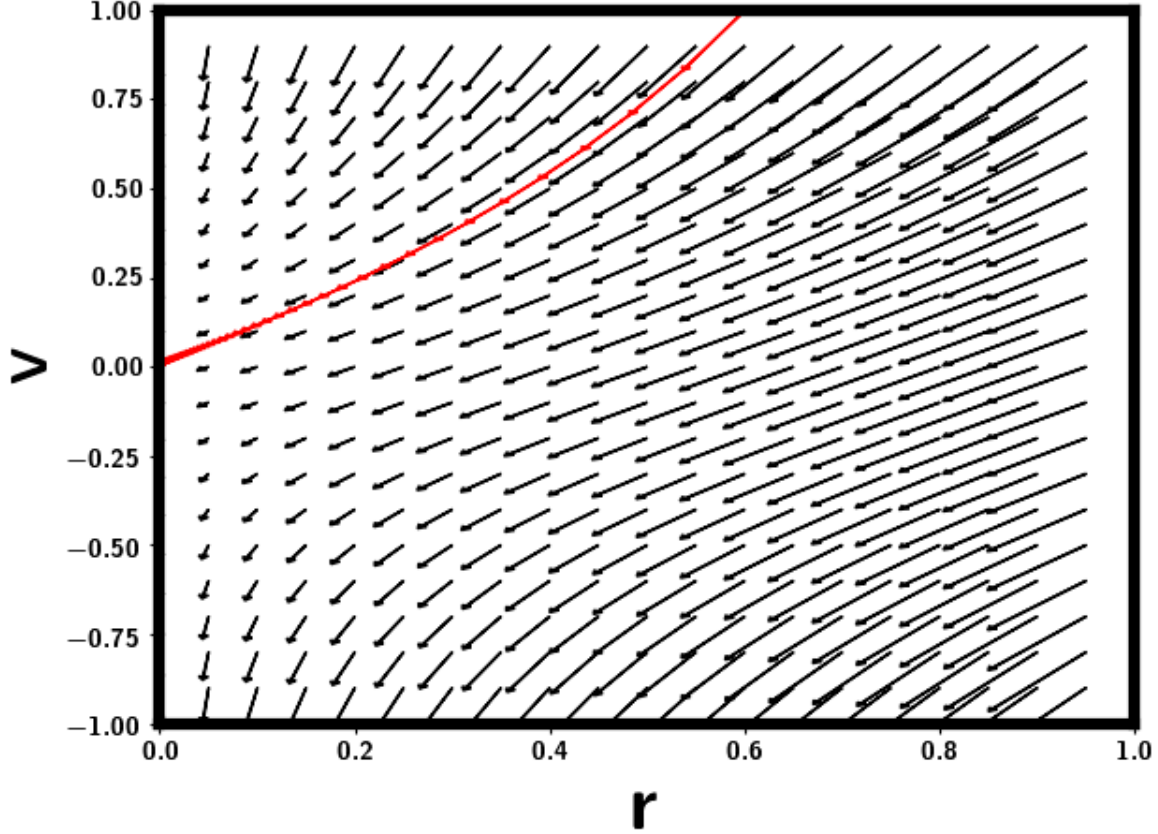


FIG. 4. RG flow in r, V parameter space at $m = 0$. There are two fixed points: $(r, V) = (0, 0)$ and $(r, V) = (0, -\infty)$.

B. Instability of the ghost Fermi surface at $m^2 > 0$

In the previous subsection, we found a stable critical ghost Fermi surface described by the fixed point at $(r, V) = (0, 0)$. The goal here is to show that this ghost Fermi surface becomes unstable to pairing immediately when we have $m^2 > 0$. As before we always assume $e_{s;0}^2 > e_{c;0}^2$.

When $m^2 > 0$, the gauge field action is

$$L_a = \frac{1}{2} \left(\frac{1}{e_{c;0}^2} \mathbf{q}^2 + \Pi_b(\omega, \mathbf{q}) + \kappa_0 \frac{|\omega|}{|\mathbf{q}|} \right) |a_1(\omega, \mathbf{q})|^2 + \frac{1}{2} \left(\frac{1}{e_{s;0}^2} \mathbf{q}^2 + \Pi_b(\omega, \mathbf{q}) + \kappa_0 \frac{|\omega|}{|\mathbf{q}|} \right) |a_S(\omega, \mathbf{q})|^2 \quad (6.11)$$

where $\Pi_b(\omega = 0, q) = |\mathbf{q}|^2 / (24\pi m)$ when $v_b |\mathbf{q}| < m$, is the Higgs boson polarizability. Let us calculate the RG flow of the BCS interaction V_s in the singlet channel. We will set a cutoff $\Lambda = m/v_b$ for $|\mathbf{q}|$. This means we first integrate out the boson field and the gauge field with $|\mathbf{q}| > m/v_b$. Then we start the RG flow from the scale m . Thus we can use the following action

for the gauge field:

$$L_a = \frac{1}{2} \left(\frac{1}{\alpha_c} \mathbf{q}^2 + \kappa_0 \frac{|\omega|}{|\mathbf{q}|} \right) |a_1(\omega, \mathbf{q})|^2 + \frac{1}{2} \left(\frac{1}{\alpha_s} \mathbf{q}^2 + \kappa_0 \frac{|\omega|}{|\mathbf{q}|} \right) |a_S(\omega, \mathbf{q})|^2 \quad (6.12)$$

where

$$\frac{1}{e_c^2} = \frac{1}{e_{c;0}^2} + \frac{1}{24\pi m} \quad , \quad \frac{1}{e_s^2} = \frac{1}{e_{s;0}^2} + \frac{1}{24\pi m}. \quad (6.13)$$

As shown in Appendix A, the RG flow is

$$\frac{dV}{d\ell} = -(\alpha_s - \alpha_c) - V^2 \quad (6.14)$$

We also have the RG flow of α_s and α_c (modified from (6.7))

$$\begin{aligned} \frac{d\alpha_c}{d\ell} &= \frac{\epsilon}{2} \alpha_c - (\alpha_c + \alpha_s) \alpha_c \\ \frac{d\alpha_s}{d\ell} &= \frac{\epsilon}{2} \alpha_s - (\alpha_c + \alpha_s) \alpha_s \end{aligned} \quad (6.15)$$

where $\epsilon = 1$.

There is a fixed line $\alpha_c + \alpha_s = \epsilon/2$. At the $m \rightarrow 0$ limit, it is easy to find that $\alpha_s(\ell = 0) - \alpha_c(\ell = 0) \sim m^2(e_{s;0}^2 - e_{c;0}^2)/(e_{s;0}^2 e_{c;0}^2) > 0$. It is also easy to verify that $d(\frac{\alpha_s}{\alpha_c})/d\ell = 0$. So we expect $\frac{\alpha_s}{\alpha_c} > 1$ at any RG time. Then, for any V_0 , $V(\ell)$ will flow to $-\infty$ at ℓ^* , suggesting a pairing scale $\Delta \sim m e^{-\ell^*}$. We find $\Delta \sim m \exp(-\pi/\sqrt{\alpha_s - \alpha_c}) \sim m \exp\left(-e_{c;0} e_{s;0}/m \sqrt{(e_{s;0}^2 - e_{c;0}^2)}\right)$. With the bare value $e_{s;0} > e_{c;0}$, we therefore find that the ghost Fermi surface is not stable to pairing even for infinitesimal small $m^2 > 0$, although the pairing scale is exponentially suppressed by a factor $m \exp(-a/m)$ as $m \rightarrow 0$.

C. Phase diagram

Based on the RG flow above, we can sketch a phase diagram as shown in Fig. 5. Depending on a parameter $g(r, V)$, we can have either a direct deconfined quantum critical point or an intermediate superconductor phase. Even in the later case, the higher temperature region may still be controlled by the DQCP.

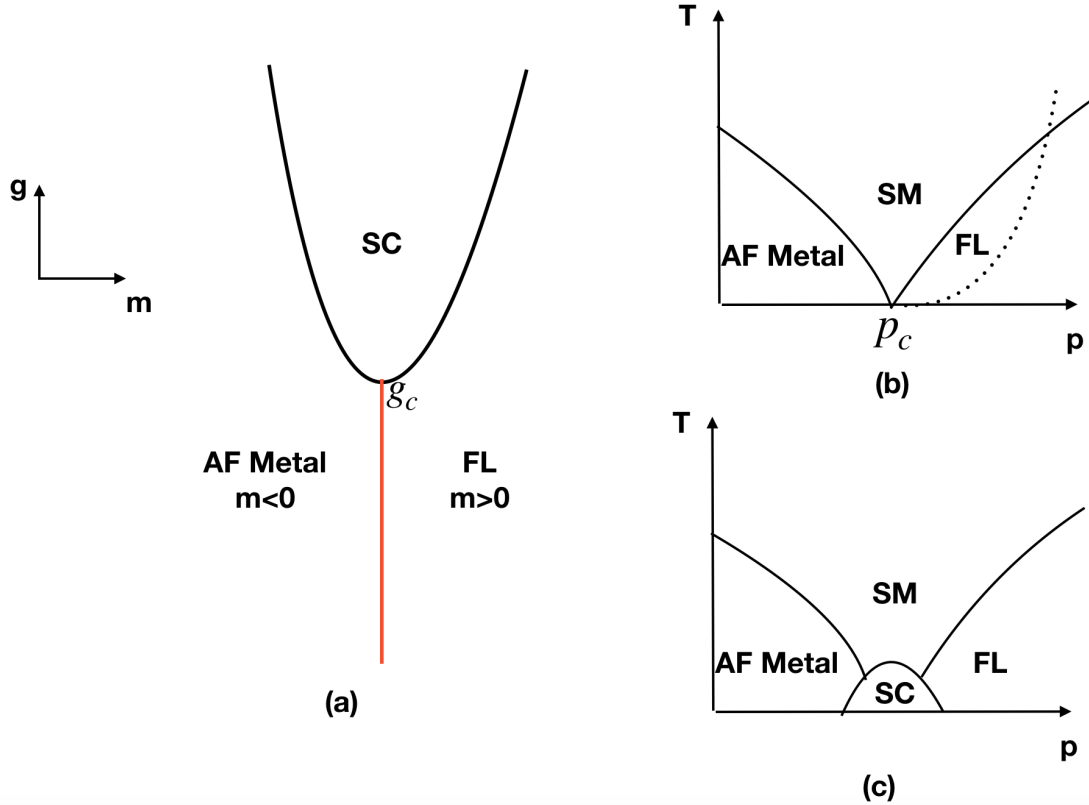


FIG. 5. A sketch of phase diagram determined by m and g , where g is a function of r, V . (a) There can be a single direct transition or there can be an intermediate superconducting phases. (b) A direct phase transition tuned by parameter p . The dashed line inside the FL indicates the exponentially small scale for the pairing of the ghost Fermi surface close to p_c . (c) There is an intermediate superconductor phase sandwiched between AF Metal and FL.

VII. HIGGS BOSON FLUCTUATIONS

This section will further discuss the Higgs boson sector for the three DQCPs. We already presented the Lagrangians L_Φ in Section VC.

First, we note that because of the $|\omega|/|\mathbf{q}|$ term in the Lagrangians of the gauge fields in (6.1,6.12), the couplings between the Higgs boson and the gauge fields are irrelevant [40, 41, 46]. This is because of the scaling dimension $[\omega] = [\mathbf{q}] = 1$ in the Higgs boson sector, and thus $|\omega|/|\mathbf{q}|$ has the same scaling dimension as a Higgs mass term m^2 . Therefore, we can drop the gauge fields in the action of the Higgs boson, and the gauge symmetries now become global symmetries for the Higgs boson Φ .

We will now comment on the additional terms in (5.1), arising from a direct coupling between the Higgs boson and fermion sectors.

For DQCP1 and DQCP2, there can be couplings like:

$$L_{\Phi C} + L_{\Phi \Psi} = g'_\beta (\Phi^\dagger \sigma^\beta \Phi) (C^\dagger \sigma^\beta C) + g_{\alpha\beta} (\Phi^\dagger \tau^\alpha \sigma^\beta \Phi) (\Psi^\dagger \tau^\alpha \sigma^\beta \Psi) \quad (7.1)$$

The bilinear $O_{\alpha\beta} = \Phi^\dagger \tau_\alpha \sigma_\beta \Phi$, with $\alpha, \beta = 0, x, y, z$, was related to various order parameters in Section VC; here, integration of fermion C or Ψ will provide a damping term

$$L'_\Phi = \frac{g_{\alpha\beta}}{v_F} \frac{|\omega|}{|\mathbf{q}|^\kappa} |O_{\alpha\beta}(\omega, \mathbf{q})|^2, \quad (7.2)$$

where $\kappa = 0, 1$ depending upon whether the order parameter is at zero or finite crystal momentum. Terms of this type have been studied elsewhere [40, 41, 43, 45, 55–59], and we leave their analysis to future work. It is expected that they are relevant, and could significantly modify the critical properties.

For DQCP3, we start from (5.11), and the fixed point of two decoupled XY transition at $\lambda_1 = 0$. Then $[\lambda_1] = 2/\nu - 3 = -0.0225$ is irrelevant. The term $L'_\Phi = (|\omega|/|\mathbf{q}|) |O(\omega, \mathbf{q})|^2$ with $O = \sum_{a=\pm} \varphi_a^\dagger \varphi_a$ has the same scaling dimension as λ_1 , and is irrelevant. We conclude that the Higgs boson sector for DQCP3 is described by a fixed point of two decoupled XY theories.

A. Universal conductivity

In this subsection, we comment on the conductivity of the Higgs boson, which is important because it enters the action of the gauge field in Section VI. For simplicity, let us organize the terms in the effective action for the gauge field as:

$$L'_\Phi[a] = \Pi_+ |a_+(\mathbf{q})|^2 + \Pi_- |a_-(\mathbf{q})|^2 + \Pi_{+-} (a_+(\mathbf{q}) a_-(\mathbf{-q}) + a_-(\mathbf{q}) a_+(\mathbf{-q})) \quad (7.3)$$

where the gauge fields a_\pm were introduced above (5.6); we view a_a with $a = \pm$ as a probe gauge field coupling to Φ_a .

Because translation symmetry T_x exchanges Φ_+ and Φ_- and thus it also exchanges a_+ and a_- , we must have $\Pi_+(\mathbf{q}) = \Pi_-(\mathbf{q})$. The crucial question is what $\Pi_{+-}(\mathbf{q})$ is. For the DQCP3, $\Pi_{+-}(\mathbf{q}) = 0$ because the two flavors are decoupled.

Next we argue that the Π_{+-} term is zero for DQCP1 and DQCP2 in perturbation theory up to second order of λ_1, λ_2 in (5.10). We can divide the interaction between the two flavors to two categories: (I) $\Phi_{+;\sigma_1}^\dagger \Phi_{+;\sigma_1} \Phi_{-;\sigma_2}^\dagger \Phi_{-;\sigma_2}$ where $\sigma_1, \sigma_2 = \uparrow, \downarrow$. (II) $\Phi_{+;\sigma}^\dagger \Phi_{+;\bar{\sigma}} \Phi_{-;\bar{\sigma}}^\dagger \Phi_{-;\sigma}$, where $\bar{\sigma}$ is the opposite spin of σ . The global $SU(2)$ spin rotation forbids other terms.

We note that there are two different charge conjugation symmetry C_a , which acts on each flavor separately. First, $C_a : \Phi_a(x) \rightarrow \Phi_a^\dagger(x)$ is a symmetry for the type I interaction. The second charge conjugation symmetry, $\tilde{C}_a : \Phi_a(x) \rightarrow \sigma_x \Phi_a^\dagger(x)$ is a symmetry for the type II interaction. If there is

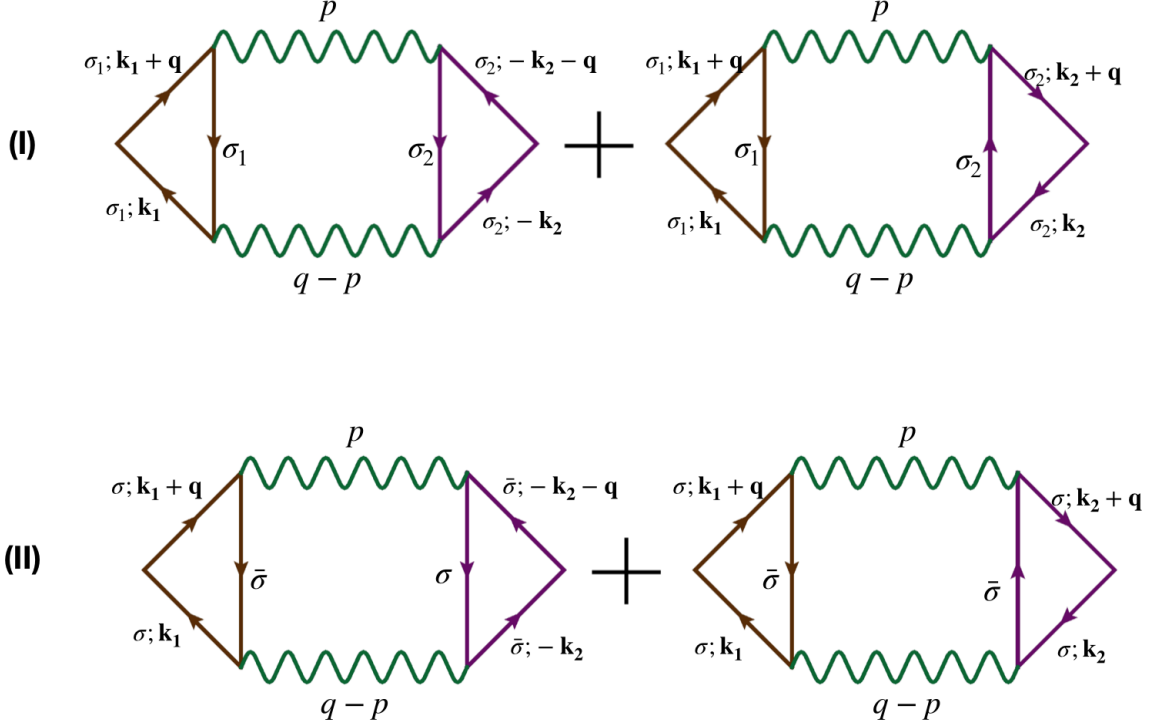


FIG. 6. Second order diagrams for $\Pi_{+-}(\mathbf{q})$. The wave line denotes the inter-flavor four fermion interaction. For each diagram, the left triangle is for Φ_+ and the right triangle is for Φ_- . The two vertexes are associated with a factor $k_{1;x}k_{2;x}$ in first diagram and $-k_{1;x}k_{2;x}$ in the second diagram. Thus the two diagrams cancel each other as long as we have $G_{\sigma_1}(\mathbf{k}) = G_{\sigma_2}(-\mathbf{k})$.

only type I interaction, then we can apply symmetry C_- , which also maps $a_-(\mathbf{q}) \rightarrow -a_-(\mathbf{q})$. This symmetry fixes $\Pi_{+-}(\mathbf{q}) = 0$. Similarly if we only have type II interaction, \tilde{C}_- fixes $\Pi_{+-}(\mathbf{q}) = 0$.

It is not clear whether both types of interaction exist at the final critical point, but even if they coexist, $\Pi_{+-}(\mathbf{q}) = 0$ up to the second order perturbation. The first order diagram always vanishes and the second-order diagram is listed in Fig. 6. Fortunately, in each diagram, only one type of interaction is involved. Hence the charge conjugation symmetry C_- or \tilde{C}_- reverse the propagator of Φ_- and guarantees the net result is zero.

At the third order, there is diagram involving both types of interaction, for example shown in Fig. 7. The diagram is generically not zero, but is expected to be small because it is at order $O(\lambda_2^3)$.

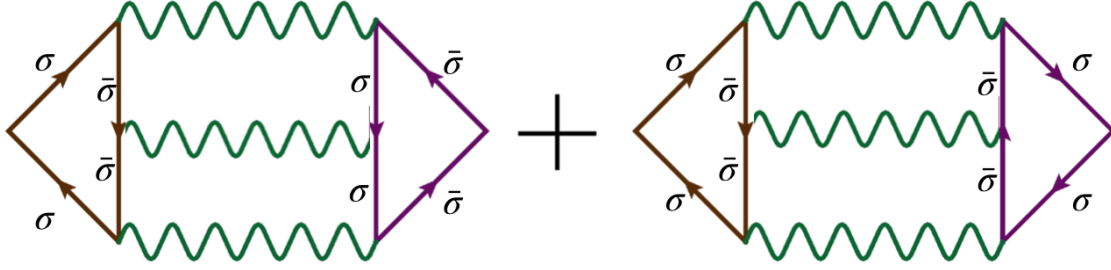


FIG. 7. A third order diagram for $\Pi_{+-}(\mathbf{q})$. The two diagrams do not cancel because $\lambda_{\sigma\sigma;\bar{\sigma}\bar{\sigma}} \neq \lambda_{\bar{\sigma}\bar{\sigma};\sigma\sigma}$, arising from the $\lambda_2(\Phi^\dagger\sigma\Phi) \cdot (\Phi^\dagger\sigma\Phi)$ term.

VIII. PROPERTY OF THE PHYSICAL FERMI SURFACE

In Sections VI and VII, we focused on the ghost Fermi surface and the Higgs boson respectively. Here we comment on the property of the physical Fermi surface formed by electron C , with an emphasis on possible non-Fermi liquid behavior. While the ghost Fermi surface dominates thermal properties, including the specific heat, as noted earlier, it is invisible to spin, charge, and photoemission probes. The charge transport will be dominated by the physical Fermi surface and it is interesting to study whether the physical Fermi surface will become non-Fermi-liquid at the critical region. We will focus on DQCP2.

There are two main effects on the physical Fermi surface: (i) the Yukawa coupling $g \sum_{a=\pm} (C^\dagger \Phi_a) \Psi_a$; (ii) the coupling to the order parameter: $g_0 \sum_i (C^\dagger C) (\Phi^\dagger \Phi) + g_s \sum_i (-1)^i (C^\dagger \sigma C) \cdot (\Phi^\dagger \tau_z \sigma \Phi) + g'_s \sum_i (C^\dagger \sigma C) \cdot (\Phi^\dagger \sigma \Phi)$.

The effect of the Yukawa coupling g depends on the Fermiology at the QCP. If the Fermi surfaces of C and Ψ do not touch each other, this coupling is irrelevant.

The coupling $g_O C^\dagger C O$ will depend on the scaling dimension of the composite order parameter O . The propagator of O will be $(\omega^2 + |\mathbf{q}|^2)^{\frac{\alpha}{2}} |O(\omega, \mathbf{q})|^2$. If $\alpha < 1$, the coupling to the order parameter is irrelevant. If $\alpha > 1$, the order parameter fluctuation can lead to non-Fermi-liquid for the physical Fermi surface [60].

IX. CONCLUSIONS

In this paper, and in our earlier work [23], we have shown that ancilla qubits are a powerful tool in resolving many long-standing issues in the theory of quantum phase transitions of correlated

metals. When studying phase transitions between states with distinct Fermi surfaces, and more so in cases where the Fermi surfaces carry distinct gauge charges, past approaches invariably made a choice of one set of Fermi surfaces about which to analyze fluctuations; this usually led to difficulties in describing ‘the order side’ of the phase transition, where the emergence of a new set of fermions was required from non-perturbative effects. The ancilla approach is more democratic, and allows one to treat both sets of Fermi surfaces within the same framework, and within perturbation theory. And subtle constraints on the relationship between Fermi surface volume [24, 25] and the bulk topological order become much easier to implement on both sides of the transition.

We have presented here a set of deconfined critical theories for the phase transitions in Fig. 2, labeled DQCP1, DQCP2, DQCP3. The matter fields of these theories are:

- Higgs fields, Φ , carrying fundamental charges of emergent gauge fields, along with unit physical electromagnetic charge, $S = 1/2$ under global spin rotations, and transformations under lattice and time-reversal symmetries.
- Ghost fermions, Ψ , which carry neither spin nor charge, and so are detectable only in energy probes.
- Fermi surface of the underlying electrons, C , which are not fractionalized in any stage of the theory.

The gauge sector had $(SU(2)_S \times U(1)_1)/Z_2$ gauge fields for DQCP1, and $(U(1)_S \times U(1)_1)/Z_2$ gauge fields for DQCP2 and DQCP3. (We contrast to other recent works for optimal doping criticality [35, 42–45], which had only a $SU(2)_S$ gauge field, and Higgs fields that were neutral under physical electromagnetism and spin.)

We also discussed some observable consequences of these DQCPs. They allow for a jump in the size of the Fermi surfaces, and a correspondingly discontinuous Hall effect. Photoemission experiments detect only the C Fermi surfaces, and these could have marginal Fermi liquid-like spectra, as discussed in Section VIII. The ghost fermions are detectable only in thermal probes, and lead to a $T \ln(1/T)$ specific heat at the DQCP, from a mechanism similar to that in Ref. 46. In the presence of disorder, the AF order near the DQCP could be replaced by glassy magnetic order. These are all phenomenologically very attractive features [50, 61–63]. We speculate that the ghost fermions also play a significant role in the anomalous thermal Hall effect observed recently [64, 65].

ACKNOWLEDGEMENTS

This research was supported by the National Science Foundation under Grant No. DMR-2002850.

Appendix A: RG flow of the ghost Fermi surface coupled to a $U(1) \times U(1)$ gauge field

At the QCP, the Higgs boson decouples, and we only need to consider the coupling between the ghost Fermi surface and the $U(1)_S \times U(1)_1$ gauge field. We consider the action

$$S = S_a + S_\Psi \quad (\text{A1})$$

with

$$S_a = \frac{1}{2} \int \frac{d\omega d^2q}{(2\pi)^3} \left[\left(\frac{1}{e_c^2} |q_y|^{1+\epsilon} + \kappa_0 \frac{|\omega|}{|q_y|} \right) |a_c(\omega, \mathbf{q})|^2 + \left(\frac{1}{e_s^2} |q_y|^{1+\epsilon} + \kappa_0 \frac{|\omega|}{|q_y|} \right) |a_s(\omega, \mathbf{q})|^2 \right] \quad (\text{A2})$$

and

$$S_\psi = \int \frac{d\omega d^2k}{(2\pi)^3} \Psi^\dagger (i\omega - v_F k_x - \kappa k_y^2) \Psi + v_F \int \frac{d^3q}{(2\pi)^3} \int \frac{d\omega d^2k}{(2\pi)^3} \Psi^\dagger(\mathbf{k} + \mathbf{q}) (a_1(\mathbf{q}) + a_S(\mathbf{q})\tau^z) \Psi(\mathbf{k}) \quad (\text{A3})$$

At the QCP, we have $\epsilon = 0$. When the Higgs boson mass is large, we have $\epsilon = 1$. We have scaling $[k_y] = \frac{1}{2}$, $[k_x] = 1$, $[\omega] = 1$, $[\Psi] = -\frac{7}{4}$, $[a] = [\alpha] = -\frac{3}{2}$, $[e_c^2] = [e_s^2] = \frac{\epsilon}{2}$, $[v_F] = 0$. Actually the only meaningful coupling is $\alpha_c = \frac{e_c^2 v_F}{4\pi^2}$ and $\alpha_s = \frac{e_s^2 v_F}{4\pi^2}$. From the naive scaling we get $[\alpha_c] = [\alpha_s] = \frac{\epsilon}{2}$. At $\epsilon = 0$ the coupling is marginal and there is hope to do controlled calculation.

Next we perform a renormalization group analysis using ϵ expansion. It is useful to introduce the redefinition:

$$\begin{aligned} \Psi_0 &= Z^{1/2} \Psi \\ v_F^0 &= Z_{v_F} v_F \\ e_c^0 &= \mu^{\frac{\epsilon}{4}} e_c Z_{e_c} \\ e_s^0 &= \mu^{\frac{\epsilon}{4}} e_s Z_{e_s} \\ a_c^0 &= Z_{a_c} a_c \\ a_s^0 &= Z_{a_s} a_s \end{aligned} \quad (\text{A4})$$

and then we can rewrite the original action as

$$\begin{aligned}
S &= \frac{1}{2} \int \frac{d\omega d^2q}{(2\pi)^3} \left[\left(\frac{Z_{a_c}^2}{\mu^{\frac{\epsilon}{2}} Z_{e_c}^2 e_c^2} |q_y|^{1+\epsilon} + Z_{a_c}^2 \kappa_0 \frac{|\omega|}{|q_y|} \right) |a_c(\omega, \mathbf{q})|^2 \right. \\
&\quad \left. + \sum_{a=1,2,3} \left(\frac{Z_{a_s}^2}{\mu^{\frac{\epsilon}{2}} Z_{e_s}^2 e_s^2} |q_y|^{1+\epsilon} + Z_{a_s}^2 \kappa_0 \frac{|\omega|}{|q_y|} \right) |\alpha_s^a(\omega, \mathbf{q})|^2 \right] \\
&\quad + \int \frac{d\omega d^2k}{(2\pi)^3} \Psi^\dagger (iZ\omega - ZZ_{v_F} v_F k_x - ZZ_{v_F} \kappa k_y^2) \Psi \\
&\quad + v_F ZZ_{v_F} \int \frac{d^3q}{(2\pi)^3} \int \frac{d\omega d^2k}{(2\pi)^3} \Psi^\dagger(\mathbf{k} + \mathbf{q}) (Z_{a_c} a_1(\mathbf{q}) + Z_{a_s} a_S(\mathbf{q}) \tau^z) \Psi(\mathbf{k}) \tag{A5}
\end{aligned}$$

From the Ward identity, we expect $Z_{a_c} = 1$ and $Z_{a_s} = 1$. Hence the fermion-gauge field vertex correction should be purely from ZZ_{v_F} . As we will see, $ZZ_{v_F} = 1$, implying that there is no vertex correction. When $\epsilon < 1$, we expect $Z_{e_c} = Z_{e_s} = 1$ because the non-analytic form $|q_y|^{1+\epsilon}$ can not be renormalized. Therefore the only important renormalization is from $Z = Z_{v_F}^{-1}$.

The fermion self-energy at one-loop order is

$$\begin{aligned}
\Sigma(i\omega) &= -\frac{e_c^2 v_F^2}{(2\pi)^3} \int dq_0 d^2q \frac{1}{|q_y|^{1+\epsilon} + \kappa_0 e_c^2 \frac{|q_0|}{|q_y|}} \frac{1}{i\omega + iq_0 - v_F(k_x + q_x) + \kappa(k_y + q_y)^2} \\
&\quad + \frac{e_s^2 v_F^2}{(2\pi)^3} \int dq_0 d^2q \frac{1}{|q_y|^{1+\epsilon} + \kappa_0 e_s^2 \frac{|q_0|}{|q_y|}} \frac{1}{i\omega + iq_0 - v_F(k_x + q_x) + \kappa(k_y + q_y)^2} \\
&= \frac{\alpha_c}{2} \int dq_0 dq_y \frac{i \operatorname{sign}(\omega + q_0)}{|q_y|^{1+\epsilon} + \kappa_0 e_c^2 \frac{|q_0|}{|q_y|}} + \frac{\alpha_s}{2} \int dq_0 dq_y \frac{i \operatorname{sign}(\omega + q_0)}{|q_y|^{1+\epsilon} + \kappa_0 e_s^2 \frac{|q_0|}{|q_y|}} \\
&= (\alpha_c + \alpha_s) \frac{1}{\epsilon} \int dq_0 i \operatorname{sign}(\omega + q_0) + \dots \\
&= 2(\alpha_c + \alpha_s) i\omega \frac{1}{\epsilon} \tag{A6}
\end{aligned}$$

In the above we only keep the divergent part $O(1/\epsilon)$. To cancel the divergent part, we need

$$Z = Z_{v_F}^{-1} = 1 - 2(\alpha_c + \alpha_s) \frac{1}{\epsilon} \tag{A7}$$

Next, we show explicitly that the vertex correction vanishes [47]. For simplicity we use a_1 as

an illustration. We have

$$\begin{aligned}
\delta\Gamma^c(p_0, p_x, p_y) &= \int \frac{dq^3}{2\pi} \frac{1}{iq_0 - v_F q_x - \kappa_0 q_y^2} \frac{1}{iq_0 + ip_0 - v_F(q_x + p_x) - \kappa_0(q_y + p_y)^2} \times \\
&\quad \left(\frac{\alpha_c v_F}{|q_y|^{1+\epsilon} + \kappa_0 e_c^2 \frac{|q_0|}{|q_y|}} + \frac{\alpha_s v_F}{|q_y|^{1+\epsilon} + \kappa_0 e_s^2 \frac{|q_0|}{|q_y|}} \right) \\
&= i \text{sign}(p_0) \int dq_y \int_0^{|p_0|} dq_0 \left(\frac{\alpha_c}{|q_y|^{1+\epsilon} + \kappa_0 e_c^2 \frac{|q_0|}{|q_y|}} + \frac{\alpha_s}{|q_y|^{1+\epsilon} + \kappa_0 e_s^2 \frac{|q_0|}{|q_y|}} \right) \times \\
&\quad \frac{1}{ip_0 - v_F p_x - 2\kappa_0 p_y q_y - \kappa_0 p_y^2} \tag{A8}
\end{aligned}$$

where (p_0, p_x, p_y) is the external momentum of the photon at the vertex. We assume that the $(\omega, k_x, k_y) = (0, 0, 0)$ for one external fermion. In the first step we integrate q_x and get a factor $\text{sign}(p_0 + q_0) - \text{sign}(q_0)$, which is equal to 2 for $q_0 \in [-p_0, 0]$ and zero elsewhere. It is easy to find that $\delta\Gamma^c(p_0, p_x, p_y) = 0$ in the $p_0 = 0$, but p_x, p_y finite limit. Thus we conclude that there is no vertex correction. The same conclusion holds for the vertex corresponding to a_S .

Finally, we can get the beta function $\beta(\alpha_c) = -d\alpha_c/d\log\mu$ and $\beta(\alpha_s) = -d\alpha_s/d\log\mu$ (note, this is the negative of the usual definition) from the relation $\alpha_c^0 = \mu^{\frac{\epsilon}{2}} \alpha Z_{e_c}^2 Z_{v_F}$ and $\alpha_s^0 = \mu^{\frac{\epsilon}{2}} \alpha Z_{e_s}^2 Z_{v_F}$. We have equations:

$$\begin{aligned}
0 &= -\frac{\epsilon}{2} + \frac{1}{\alpha_c} \beta(\alpha_c) + \frac{2}{Z_{e_c}} \left(\frac{\partial Z_{e_c}}{\partial \alpha_c} \beta(\alpha_c) + \frac{\partial Z_{e_c}}{\partial \alpha_s} \beta(\alpha_s) \right) + \frac{1}{Z_{v_F}} \left(\frac{\partial Z_{v_F}}{\partial \alpha_c} \beta(\alpha_c) + \frac{\partial Z_{v_F}}{\partial \alpha_s} \beta(\alpha_s) \right) \\
0 &= -\frac{\epsilon}{2} + \frac{1}{\alpha_s} \beta(\alpha_s) + \frac{2}{Z_{e_s}} \left(\frac{\partial Z_{e_s}}{\partial \alpha_c} \beta(\alpha_c) + \frac{\partial Z_{e_s}}{\partial \alpha_s} \beta(\alpha_s) \right) + \frac{1}{Z_{v_F}} \left(\frac{\partial Z_{v_F}}{\partial \alpha_c} \beta(\alpha_c) + \frac{\partial Z_{v_F}}{\partial \alpha_s} \beta(\alpha_s) \right) \tag{A9}
\end{aligned}$$

The above equations can be written as:

$$\begin{aligned}
\left[\frac{1}{\alpha_c} + \frac{2}{\epsilon + 2(\alpha_c + \alpha_s)} \right] \beta(\alpha_c) + \frac{2}{\epsilon + 2(\alpha_c + \alpha_s)} \beta(\alpha_s) &= \frac{\epsilon}{2} \\
\frac{2}{\epsilon + 2(\alpha_c + \alpha_s)} \beta(\alpha_c) + \left[\frac{1}{\alpha_s} + \frac{2}{\epsilon + 2(\alpha_c + \alpha_s)} \right] \beta(\alpha_s) &= \frac{\epsilon}{2} \tag{A10}
\end{aligned}$$

The solution is

$$\begin{aligned}
\beta(\alpha_c) &= \frac{\epsilon}{2} \alpha_c - \alpha_c(\alpha_c + \alpha_s) \\
\beta(\alpha_s) &= \frac{\epsilon}{2} \alpha_s - \alpha_s(\alpha_c + \alpha_s) \tag{A11}
\end{aligned}$$

At the QCP, we expect $\alpha_c(\ell = 0) = \alpha_s(\ell = 0) = 1/\sigma_b$. Here $\ell = -\log\mu$ is the time of the RG flow. Then according to the above RG flow, $\alpha_c = \alpha_s$ will remain true for any ℓ . In the $\ell \rightarrow \infty$ limit we reach the fixed point $\alpha_c = \alpha_s = 0$. As usual the fermion self energy has a log correction $i\omega \log\omega$ and the specific heat C/T from the ghost fermion also has a log T correction.

Appendix B: Pairing instability for the FL*-FL transition with $U(2)$ gauge theory

We can easily generalize the calculation in Appendix A for the $U(1)_S \times U(1)_1$ gauge theory of DQCP2 and DQCP3 to the $SU(2)_S \times U(1)_1$ theory for DQCP1 of the FL*-FL transition. The main change is that the a_S gauge field now has 3 components a_S^α , $\alpha = x, y, z$. This has the consequence that the fermion self energy in (A6) is modified to

$$\begin{aligned}
\Sigma(i\omega) &= -\frac{e_c^2 v_F^2}{(2\pi)^3} \int dq_0 d^2 q \frac{1}{|q_y|^{1+\epsilon} + \kappa_0 e_c^2 \frac{|q_0|}{|q_y|}} \frac{1}{i\omega + iq_0 - v_F(k_x + q_x) + \kappa(k_y + q_y)^2} \\
&+ \frac{3e_s^2 v_F^2}{(2\pi)^3} \int dq_0 d^2 q \frac{1}{|q_y|^{1+\epsilon} + \kappa_0 e_s^2 \frac{|q_0|}{|q_y|}} \frac{1}{i\omega + iq_0 - v_F(k_x + q_x) + \kappa(k_y + q_y)^2} \\
&= \frac{\alpha_c}{2} \int dq_0 dq_y \frac{i \operatorname{sign}(\omega + q_0)}{|q_y|^{1+\epsilon} + \kappa_0 e_c^2 \frac{|q_0|}{|q_y|}} + \frac{3\alpha_s}{2} \int dq_0 dq_y \frac{i \operatorname{sign}(\omega + q_0)}{|q_y|^{1+\epsilon} + \kappa_0 e_s^2 \frac{|q_0|}{|q_y|}} \\
&= (\alpha_c + 3\alpha_s) \frac{1}{\epsilon} \int dq_0 i \operatorname{sign}(\omega + q_0) + \dots \\
&= 2(\alpha_c + 3\alpha_s) i\omega \frac{1}{\epsilon}
\end{aligned} \tag{B1}$$

In the above, an additional factor of 3 before α_s is needed because we sum over the three components a_S^α . In the fourth line we only keep the divergent part $O(\frac{1}{\epsilon})$. So the renormalization factors in (A7) are replaced by

$$Z = Z_{v_F}^{-1} = 1 - 2(\alpha_c + 3\alpha_s) \frac{1}{\epsilon}. \tag{B2}$$

Following the procedure in Appendix A, we now obtain the β functions replacing (A11)

$$\begin{aligned}
\beta(\alpha_c) &= \frac{\epsilon}{2} \alpha_c - \alpha_c(\alpha_c + 3\alpha_s) \\
\beta(\alpha_s) &= \frac{\epsilon}{2} \alpha_s - \alpha_s(\alpha_c + 3\alpha_s).
\end{aligned} \tag{B3}$$

At the QCP, at one-loop order in the Higgs boson fluctuations $\alpha_c(\ell = 0) = \alpha_s(\ell = 0) = 1/\sigma_b$. However, we don't expect this equality to be obeyed at higher loops, because the $SU(2)_S$ and $U(1)_1$ sectors will behave differently. Nevertheless, it is easy to check from (B3) that $\alpha_c/\alpha_s = r$ does not flow with ℓ .

Then according to the above RG flow, $\alpha_c = \alpha_s$ will remain true for any ℓ .

1. Pairing instability

The leading contribution to interaction in BCS channel for ghost Fermi surface Ψ is from exchange of one photon or gluon. Generically, it is in the form:

$$S_{BCS} = \int d^2k_i d\omega_i \psi_a^\dagger(k_1) \psi_b^\dagger(-k_1) \psi_d(-k_2) \psi_c(k_2) [V_a(\delta_{ac}\delta_{bd} + \delta_{ad}\delta_{bc}) + V_s(\delta_{ac}\delta_{bd} - \delta_{ad}\delta_{bc})] F(k_1 - k_2) \quad (\text{B4})$$

Here V_a is the pairing with odd angular momentum and V_s is the pairing with even angular momentum. $F(q = k_1 - k_2)$ is coming from the integration of the propagator of the photon or gluon.

Next, we decide the contribution from the $U(1)$ gauge field a_1 and $SU(2)$ gauge field a_S . The contribution is proportional to $\sum_\alpha t_{ac}^\alpha t_{bd}^\alpha$, where t^α are the corresponding generators. For the $U(1)$ gauge field, we just have $t = I$ and $\sum_\alpha t_{ac}^\alpha t_{bd}^\alpha = \delta_{ac}\delta_{bd}$. Thus we can get $V_a = V_s = \frac{1}{2}$. For the $SU(2)$ gauge field, one finds that $V_a = \frac{1}{2}$ and $V_s = -\frac{3}{2}$. If we sum up the contributions from a_1 and a_S , V_a is always positive, but V_s can be negative.

So we obtain the following flow equation in the even angular momentum sector

$$\frac{dV_s}{d\ell} = \frac{1}{2}\alpha_c - \frac{3}{2}\alpha_s - V_s^2 \quad (\text{B5})$$

Using the ℓ independence of $r = \alpha_c(\ell)/\alpha_s(\ell)$, at the quantum-critical point ($\epsilon = 0$) the RG flow equations become

$$\begin{aligned} \frac{dV_s}{d\ell} &= -\frac{(3-r)}{2}\alpha_s - V_s^2 \\ \frac{d\alpha_s}{d\ell} &= -(3+r)\alpha_s^2 \end{aligned} \quad (\text{B6})$$

There is a fixed point $(\alpha, V_s) = (0, 0)$. The stability of this fixed point now depends upon whether $3 - r$ is negative or positive [27, 48]. The value of r depends upon the ratio of the $SU(2)_S$ and $U(1)_1$ conductivities of critical boson theory. At one loop, the conductivities are equal, and so $r = 1$. For the XY model, it is known that the exact conductivity is only about 10% smaller than the one loop result [52, 53]. So it is highly unlikely that $r > 3$ (in which case there is a regime where the fixed point, and the critical Fermi surface, is stable). We therefore consider the case $r < 3$ in more detail, where we show that this fixed point is unstable to infinitesimal α . First, we have the solution for α :

$$\alpha_s(\ell) = \frac{1}{1/\alpha_0 + (3+r)\ell} \quad (\text{B7})$$

Then we assume $((3-r)/2)\alpha_s(\ell=0) = \alpha_0 \ll 1$, then in the range $\ell \ll 1/(\alpha_0)$, we can use the following equation:

$$\frac{dV_s}{d\ell} = -\alpha_0 - V_s^2 \quad (\text{B8})$$

with the solution $V_s(\ell) = -\sqrt{\alpha_0} \tan(\sqrt{\alpha_0}\ell - C)$. Even for $V_s(\ell = 0) = +\infty$, $V_s(\ell)$ will flow to $-\infty$ before $\ell^* = \pi/\sqrt{\alpha_0} \ll 1/\alpha_0$, which justifies the assumption to use $\alpha(\ell) = \alpha_0$ in the $\alpha_0 \ll 1$ limit. The pairing scale is $\Delta \sim \Lambda e^{-\pi/\sqrt{\alpha_0}}$.

The DQCP can be stabilized by adding magnetic field B . Because of the large diamagnetism of the Higgs boson Φ , which couples to both A and a_1 . It is favored to lock the internal flux to the external magnetic field: $da_1 = B$. As a result, the ghost Fermi surface Ψ also feels an effective magnetic field and the superconducting instability can be suppressed. Above a critical magnetic field B_c , we expect to see a direct transition between the FL* and FL. Of course in this case the ghost Fermi surface should also survive for a while after the transition.

Appendix C: Relation to Hertz-Millis theory

Here we want to comment on the relation between DQCP2 and the conventional Hertz-Millis theory [12, 13]. In principle the two phases separated by these two QCPs are the same. The DQCP2 provides an example of a beyond Landau theory for a Landau allowed phase transition.

In our theory, the DQCP2 is actually a critical line specified by a parameter M_1 , which controls the size of the ghost Fermi surface. If we increase $M_1 > M_{1;c}$, the ghost Fermi surface size becomes zero. In this case, we now show that our DQCP2 will reduce to the conventional Hertz-Millis theory.

When $M_1 > M_{1;c}$, Ψ is gapped out by the M_1 term. Then Φ_+ and Φ_- are two CP¹ QED theories, which are equivalent to two 3D $O(3)$ theories if there are no crossing terms between Φ_+ and Φ_- . Because of the monopole operator, Φ is confined and the critical theory should be formed by gauge invariant operator. By defining $\mathbf{n}_+ = \Phi_+^\dagger \boldsymbol{\sigma} \Phi_+$ and $\mathbf{n}_- = \Phi_-^\dagger \boldsymbol{\sigma} \Phi_-$, we can use (5.10) to write the Lagrangian as:

$$L_{\mathbf{n}} = |\partial_\mu \mathbf{n}_c|^2 + m_c^2 |\mathbf{n}_c|^2 + |\partial_\mu \mathbf{n}_s|^2 + m_s^2 |\mathbf{n}_s|^2 + \lambda_c |\mathbf{n}_c|^4 + \lambda_s |\mathbf{n}_s|^4 + \lambda_1 |\mathbf{n}_c|^2 |\mathbf{n}_s|^2 + \lambda_2 |\mathbf{n}_c \cdot \mathbf{n}_s|^2 + L'_\Phi \quad (\text{C1})$$

where $\mathbf{n}_c = \mathbf{n}_+ + \mathbf{n}_-$ and $\mathbf{n}_s = \mathbf{n}_+ - \mathbf{n}_-$. The damping term L'_Φ is as in (7.2). The translation T_x transforms as $\mathbf{n}_1 \leftrightarrow \mathbf{n}_2$ and thus $\mathbf{n}_c \rightarrow \mathbf{n}_c$ and $\mathbf{n}_s \rightarrow -\mathbf{n}_s$. As a result there is no term like $\mathbf{n}_c \cdot \mathbf{n}_s$. Physically we can view \mathbf{n}_c as FM order parameter and \mathbf{n}_s as AF order parameter.

In principle \mathbf{n}_c and \mathbf{n}_s can be disordered at different couplings. For example, we can have a critical point where m_s^2 goes to zero while $m_c^2 > 0$. This is just the conventional Hertz-Millis theory for an antiferromagnetic critical point. One can also add the CDW order parameter $\Phi^\dagger \tau_z \Phi$ to the critical theory. The point is that only one order parameter can condense now without fine tuning. Thus the DQCP2 will be reduced to the conventional symmetry breaking transition corresponding

to AF, FM or CDW order.

-
- [1] G. R. Stewart, “Non-Fermi-liquid behavior in d - and f -electron metals,” *Rev. Mod. Phys.* **73**, 797 (2001).
 - [2] P. Coleman and A. J. Schofield, “Quantum criticality,” *Nature* **433**, 226 (2005), [arXiv:cond-mat/0503002 \[cond-mat.str-el\]](#).
 - [3] H. v. Löhneysen, A. Rosch, M. Vojta, and P. Wölfle, “Fermi-liquid instabilities at magnetic quantum phase transitions,” *Rev. Mod. Phys.* **79**, 1015 (2007).
 - [4] P. Gegenwart, Q. Si, and F. Steglich, “Quantum criticality in heavy-fermion metals,” *Nature Physics* **4**, 186 (2008), [arXiv:0712.2045 \[cond-mat.str-el\]](#).
 - [5] T. Senthil, S. Sachdev, and M. Vojta, “Quantum phase transitions out of the heavy Fermi liquid,” *Physica B Condensed Matter* **359**, 9 (2005), [arXiv:cond-mat/0409033 \[cond-mat.str-el\]](#).
 - [6] S. Kirchner, S. Paschen, Q. Chen, S. Wirth, D. Feng, J. D. Thompson, and Q. Si, “Colloquium: Heavy-electron quantum criticality and single-particle spectroscopy,” *Rev. Mod. Phys.* **92**, 011002 (2020).
 - [7] C. Proust and L. Taillefer, “The Remarkable Underlying Ground States of Cuprate Superconductors,” *Annual Review of Condensed Matter Physics* **10**, 409 (2019), [arXiv:1807.05074 \[cond-mat.supr-con\]](#).
 - [8] N. P. Armitage, P. Fournier, and R. L. Greene, “Progress and perspectives on electron-doped cuprates,” *Rev. Mod. Phys.* **82**, 2421 (2010).
 - [9] A. Damascelli, Z. Hussain, and Z.-X. Shen, “Angle-resolved photoemission studies of the cuprate superconductors,” *Rev. Mod. Phys.* **75**, 473 (2003).
 - [10] L. Jiao, M. Smidman, Y. Kohama, Z. S. Wang, D. Graf, Z. F. Weng, Y. J. Zhang, A. Matsuo, E. D. Bauer, H. Lee, S. Kirchner, J. Singleton, K. Kindo, J. Wosnitza, F. Steglich, J. D. Thompson, and H. Q. Yuan, “Enhancement of the effective mass at high magnetic fields in CeRhIn₅,” *Phys. Rev. B* **99**, 045127 (2019).
 - [11] S. Seo, E. Park, E. D. Bauer, F. Ronning, J. N. Kim, J. H. Shim, J. D. Thompson, and T. Park, “Controlling superconductivity by tunable quantum critical points,” *Nature Communications* **6**, 6433 (2015).
 - [12] J. A. Hertz, “Quantum critical phenomena,” *Phys. Rev. B* **14**, 1165 (1976).
 - [13] A. J. Millis, “Effect of a nonzero temperature on quantum critical points in itinerant fermion systems,” *Phys. Rev. B* **48**, 7183 (1993).
 - [14] S. Friedemann, T. Westerkamp, M. Brando, N. Oeschler, S. Wirth, P. Gegenwart, C. Krellner, C. Geibel, and F. Steglich, “Detaching the antiferromagnetic quantum critical point from the Fermi-

surface reconstruction in YbRh_2Si_2 ,” *Nature Physics* **5**, 465 (2009).

- [15] A. Schröder, G. Aeppli, R. Coldea, M. Adams, O. Stockert, H. v. Löhneysen, E. Bucher, R. Ramazashvili, and P. Coleman, “Onset of antiferromagnetism in heavy-fermion metals,” *Nature* **407**, 351 (2000).
- [16] O. Trovarelli, C. Geibel, S. Mederle, C. Langhammer, F. M. Grosche, P. Gegenwart, M. Lang, G. Sparn, and F. Steglich, “ YbRh_2Si_2 : Pronounced Non-Fermi-Liquid Effects above a Low-Lying Magnetic Phase Transition,” *Phys. Rev. Lett.* **85**, 626 (2000).
- [17] T. Senthil, A. Vishwanath, L. Balents, S. Sachdev, and M. P. A. Fisher, “Deconfined Quantum Critical Points,” *Science* **303**, 1490 (2004), [arXiv:cond-mat/0311326 \[cond-mat.str-el\]](#).
- [18] T. Senthil, L. Balents, S. Sachdev, A. Vishwanath, and M. P. A. Fisher, “Quantum criticality beyond the Landau-Ginzburg-Wilson paradigm,” *Phys. Rev. B* **70**, 144407 (2004), [arXiv:cond-mat/0312617 \[cond-mat.str-el\]](#).
- [19] P. Coleman, C. Pépin, Q. Si, and R. Ramazashvili, “Topical Review: How do Fermi liquids get heavy and die?” *Journal of Physics Condensed Matter* **13**, R723 (2001), [arXiv:cond-mat/0105006 \[cond-mat.str-el\]](#).
- [20] K.-Y. Yang, T. M. Rice, and F.-C. Zhang, “Phenomenological theory of the pseudogap state,” *Phys. Rev. B* **73**, 174501 (2006), [arXiv:cond-mat/0602164 \[cond-mat.supr-con\]](#).
- [21] N. J. Robinson, P. D. Johnson, T. M. Rice, and A. M. Tsvelik, “Anomalies in the pseudogap phase of the cuprates: competing ground states and the role of umklapp scattering,” *Reports on Progress in Physics* **82**, 126501 (2019), [arXiv:1906.09005 \[cond-mat.supr-con\]](#).
- [22] D. G. Joshi, C. Li, G. Tarnopolsky, A. Georges, and S. Sachdev, “Deconfined critical point in a doped random quantum Heisenberg magnet,” *Phys. Rev. X* **10**, 021033 (2020), [arXiv:1912.08822 \[cond-mat.str-el\]](#).
- [23] Y.-H. Zhang and S. Sachdev, “From the pseudogap metal to the Fermi liquid using ancilla qubits,” *Phys. Rev. Research* **2**, 023172 (2020), [arXiv:2001.09159 \[cond-mat.str-el\]](#).
- [24] T. Senthil, M. Vojta, and S. Sachdev, “Weak magnetism and non-Fermi liquids near heavy-fermion critical points,” *Phys. Rev. B* **69**, 035111 (2004), [arXiv:cond-mat/0305193 \[cond-mat.str-el\]](#).
- [25] A. Paramekanti and A. Vishwanath, “Extending Luttinger’s theorem to Z_2 fractionalized phases of matter,” *Phys. Rev. B* **70**, 245118 (2004), [arXiv:cond-mat/0406619 \[cond-mat.str-el\]](#).
- [26] T. Senthil, S. Sachdev, and M. Vojta, “Fractionalized Fermi Liquids,” *Phys. Rev. Lett.* **90**, 216403 (2003), [arXiv:cond-mat/0209144](#).
- [27] L. Zou and D. Chowdhury, “Deconfined metallic quantum criticality: a $U(2)$ gauge theoretic approach,” (2020), [arXiv:2002.02972 \[cond-mat.str-el\]](#).
- [28] L. Zou and D. Chowdhury, “Deconfined Metal-Insulator Transitions in Quantum Hall Bilayers,” (2020), [arXiv:2004.14391 \[cond-mat.str-el\]](#).

- [29] Q. Si, S. Rabello, K. Ingersent, and J. L. Smith, “Locally critical quantum phase transitions in strongly correlated metals,” *Nature* **413**, 804 (2001), [arXiv:cond-mat/0011477 \[cond-mat.str-el\]](#).
- [30] Z. Bi, E. Lake, and T. Senthil, “Landau ordering phase transitions beyond the Landau paradigm,” *Phys. Rev. Research* **2**, 023031 (2020), [arXiv:1910.12856 \[cond-mat.str-el\]](#).
- [31] Z. Bi and T. Senthil, “Adventure in Topological Phase Transitions in 3+1-D: Non-Abelian Deconfined Quantum Criticalities and a Possible Duality,” *Phys. Rev. X* **9**, 021034 (2019), [arXiv:1808.07465 \[cond-mat.str-el\]](#).
- [32] P. A. Lee, N. Nagaosa, and X.-G. Wen, “Doping a Mott insulator: Physics of high-temperature superconductivity,” *Rev. Mod. Phys.* **78**, 17 (2006), [arXiv:cond-mat/0410445 \[cond-mat.str-el\]](#).
- [33] S. Sachdev, M. A. Metlitski, Y. Qi, and C. Xu, “Fluctuating spin density waves in metals,” *Phys. Rev. B* **80**, 155129 (2009), [arXiv:0907.3732 \[cond-mat.str-el\]](#).
- [34] C. Xu and S. Sachdev, “Majorana Liquids: The Complete Fractionalization of the Electron,” *Phys. Rev. Lett.* **105**, 057201 (2010), [arXiv:1004.5431 \[cond-mat.str-el\]](#).
- [35] S. Sachdev, “Topological order, emergent gauge fields, and Fermi surface reconstruction,” *Rept. Prog. Phys.* **82**, 014001 (2019), [arXiv:1801.01125 \[cond-mat.str-el\]](#).
- [36] P. Ghaemi and T. Senthil, “Néel order, quantum spin liquids, and quantum criticality in two dimensions,” *Phys. Rev. B* **73**, 054415 (2006), [arXiv:cond-mat/0509073 \[cond-mat.str-el\]](#).
- [37] R. Boyack, A. Rayyan, and J. Maciejko, “Deconfined criticality in the QED₃ Gross-Neveu-Yukawa model: The 1/N expansion revisited,” *Phys. Rev. B* **99**, 195135 (2019), [arXiv:1812.02720 \[cond-mat.str-el\]](#).
- [38] L. Janssen, W. Wang, M. M. Scherer, Z. Y. Meng, and X. Y. Xu, “Confinement transition in the QED₃-Gross-Neveu-XY universality class,” (2020), [arXiv:2003.01722 \[cond-mat.str-el\]](#).
- [39] E. Dupuis, M. Paranjape, and W. Witczak-Krempa, “Monopole operators and their symmetries in QED₃-Gross-Neveu models,” (2019), [arXiv:1911.05802 \[cond-mat.str-el\]](#).
- [40] T. Grover and T. Senthil, “Quantum phase transition from an antiferromagnet to a spin liquid in a metal,” *Phys. Rev. B* **81**, 205102 (2010), [arXiv:0910.1277 \[cond-mat.str-el\]](#).
- [41] R. K. Kaul, M. A. Metlitski, S. Sachdev, and C. Xu, “Destruction of Néel order in the cuprates by electron doping,” *Phys. Rev. B* **78**, 045110 (2008), [arXiv:0804.1794 \[cond-mat.str-el\]](#).
- [42] D. Chowdhury and S. Sachdev, “Higgs criticality in a two-dimensional metal,” *Phys. Rev. B* **91**, 115123 (2015), [arXiv:1412.1086 \[cond-mat.str-el\]](#).
- [43] S. Sachdev, H. D. Scammell, M. S. Scheurer, and G. Tarnopolsky, “Gauge theory for the cuprates near optimal doping,” *Phys. Rev. B* **99**, 054516 (2019), [arXiv:1811.04930 \[cond-mat.str-el\]](#).
- [44] H. D. Scammell, K. Patekar, M. S. Scheurer, and S. Sachdev, “Phases of SU(2) gauge theory with multiple adjoint Higgs fields in 2+1 dimensions,” *Phys. Rev. B* **101**, 205124 (2020), [arXiv:1912.06108 \[cond-mat.str-el\]](#).

- [45] H. D. Scammell, M. S. Scheurer, and S. Sachdev, “Bilocal quantum criticality,” (2020), arXiv, to appear.
- [46] T. Senthil, “Theory of a continuous Mott transition in two dimensions,” *Phys. Rev. B* **78**, 045109 (2008), arXiv:0804.1555 [cond-mat.str-el].
- [47] D. F. Mross, J. McGreevy, H. Liu, and T. Senthil, “A controlled expansion for certain non-Fermi liquid metals,” *Phys. Rev. B* **82**, 045121 (2010), arXiv:1003.0894 [cond-mat.str-el].
- [48] M. A. Metlitski, D. F. Mross, S. Sachdev, and T. Senthil, “Are non-Fermi-liquids stable to Cooper pairing?” *Phys. Rev. B* **91**, 115111 (2015), arXiv:1403.3694 [cond-mat.str-el].
- [49] J. Loram, J. Luo, J. Cooper, W. Liang, and J. Tallon, “Evidence on the pseudogap and condensate from the electronic specific heat,” *Journal of Physics and Chemistry of Solids* **62**, 59 (2001).
- [50] B. Michon, C. Girod, S. Badoux, J. Kačmarčík, Q. Ma, M. Dragomir, H. A. Dabkowska, B. D. Gaulin, J. S. Zhou, S. Pyon, T. Takayama, H. Takagi, S. Verret, N. Doiron-Leyraud, C. Marcenat, L. Taillefer, and T. Klein, “Thermodynamic signatures of quantum criticality in cuprate superconductors,” *Nature* **567**, 218 (2019), arXiv:1804.08502 [cond-mat.supr-con].
- [51] J. L. Tallon, J. G. Storey, J. R. Cooper, and J. W. Loram, “Locating the pseudogap closing point in cuprate superconductors: absence of entrant or reentrant behavior,” (2019), arXiv:1907.12018 [cond-mat.supr-con].
- [52] E. Katz, S. Sachdev, E. S. Srensen, and W. Witczak-Krempa, “Conformal field theories at nonzero temperature: Operator product expansions, Monte Carlo, and holography,” *Phys. Rev. B* **90**, 245109 (2014), arXiv:1409.3841 [cond-mat.str-el].
- [53] S. M. Chester, W. Landry, J. Liu, D. Poland, D. Simmons-Duffin, N. Su, and A. Vichi, “Carving out OPE space and precise $O(2)$ model critical exponents,” (2019), arXiv:1912.03324 [hep-th].
- [54] R. Fazio and D. Zappalà, “ ϵ expansion of the conductivity at the superconductor-Mott-insulator transition,” *Phys. Rev. B* **53**, R8883 (1996).
- [55] S. Sachdev and T. Morinari, “Strongly coupled quantum criticality with a Fermi surface in two dimensions: Fractionalization of spin and charge collective modes,” *Phys. Rev. B* **66**, 235117 (2002), arXiv:cond-mat/0207167 [cond-mat.str-el].
- [56] Z. Nussinov and J. Zaanen, “Stripe fractionalization I: the generation of Ising local symmetry,” *J. Phys. IV France* **12**, 245 (2002), cond-mat/0209437.
- [57] J. Zaanen and Z. Nussinov, “Stripe fractionalization: the quantum spin nematic and the Abrikosov lattice,” *Phys. Stat. Sol. B* **236**, 332 (2003), cond-mat/0209441.
- [58] D. F. Mross and T. Senthil, “Theory of a Continuous Stripe Melting Transition in a Two-Dimensional Metal: A Possible Application to Cuprate Superconductors,” *Phys. Rev. Lett.* **108**, 267001 (2012), arXiv:1201.3358 [cond-mat.str-el].
- [59] D. F. Mross and T. Senthil, “Stripe melting and quantum criticality in correlated metals,” *Phys.*

Rev. B **86**, 115138 (2012), [arXiv:1207.1442 \[cond-mat.str-el\]](#).

- [60] Y. Xu, H. Geng, X.-C. Wu, C.-M. Jian, and C. Xu, “Non-Landau Quantum Phase Transitions and nearly-Marginal non-Fermi Liquid,” (2019), [arXiv:1911.08503 \[cond-mat.str-el\]](#).
- [61] S. Badoux, W. Tabis, F. Laliberté, G. Grissonnanche, B. Vignolle, D. Vignolles, J. Béard, D. A. Bonn, W. N. Hardy, R. Liang, N. Doiron-Leyraud, L. Taillefer, and C. Proust, “Change of carrier density at the pseudogap critical point of a cuprate superconductor,” *Nature* **531**, 210 (2016), [arXiv:1511.08162 \[cond-mat.supr-con\]](#).
- [62] M. Frachet, I. Vinograd, R. Zhou, S. Benhabib, S. Wu, H. Mayaffre, S. Krämer, S. K. Ramakrishna, A. Reyes, J. Debray, T. Kurosawa, N. Momono, M. Oda, S. Komiya, S. Ono, M. Horio, J. Chang, C. Proust, D. LeBoeuf, and M.-H. Julien, “Hidden magnetism at the pseudogap critical point of a high temperature superconductor,” (2019), [arXiv:1909.10258 \[cond-mat.supr-con\]](#).
- [63] T. J. Reber, X. Zhou, N. C. Plumb, S. Parham, J. A. Waugh, Y. Cao, Z. Sun, H. Li, Q. Wang, J. S. Wen, Z. J. Xu, G. Gu, Y. Yoshida, H. Eisaki, G. B. Arnold, and D. S. Dessau, “A unified form of low-energy nodal electronic interactions in hole-doped cuprate superconductors,” *Nature Communications* **10**, 5737 (2019), [arXiv:1509.01611 \[cond-mat.str-el\]](#).
- [64] G. Grissonnanche, A. Legros, S. Badoux, E. Lefrançois, V. Zlatko, M. Lizaire, F. Laliberté, A. Gourgout, J. S. Zhou, S. Pyon, T. Takayama, H. Takagi, S. Ono, N. Doiron-Leyraud, and L. Taillefer, “Giant thermal Hall conductivity in the pseudogap phase of cuprate superconductors,” *Nature* **571**, 376 (2019), [arXiv:1901.03104 \[cond-mat.supr-con\]](#).
- [65] G. Grissonnanche, S. Thériault, A. Gourgout, M.-E. Boulanger, E. Lefrançois, A. Ataei, F. Laliberté, M. Dion, J.-S. Zhou, S. Pyon, T. Takayama, H. Takagi, N. Doiron-Leyraud, and L. Taillefer, “Phonons become chiral in the pseudogap phase of cuprates,” (2020), [arXiv:2003.00111 \[cond-mat.supr-con\]](#).